Leg 187 Preliminary Report

Mantle Reservoirs and Migration Associated with Australian Antarctic Rifting

Shipboard Scientific Party

Ocean Drilling Program
Texas A&M University
1000 Discovery Drive
College Station TX 77845-9547
USA

April 2000

This report was prepared from shipboard files by scientists who participated in the cruise. The report was assembled under time constraints and does not contain all works and findings that will appear in the *Initial Reports* of the ODP *Proceedings.* Reference to this report should be made as follows:

Shipboard Scientific Party, 2000. Leg 187 Preliminary Report: Mantle Reservoirs and Migration Associated with Australian Antarctic Rifting. *ODP Prelim. Rpt.,* 87 [Online]. Available from World Wide Web: <http://www-odp.tamu.edu/publications/prelim/187_prel/187prel.pdf>. [Cited YYYY-MM-DD]

Distribution

Electronic copies of this series may be obtained from the Ocean Drilling Program's World Wide Web site at http://www-odp.tamu.edu/publications.

DISCLAIMER

This publication was prepared by the Ocean Drilling Program, Texas A&M University, as an account of work performed under the international Ocean Drilling Program, which is managed by Joint Oceanographic Institutions, Inc., under contract with the National Science Foundation. Funding for the program is provided by the following agencies:

Australia/Canada/Chinese Taipei/Korea Consortium for Ocean Drilling
Deutsche Forschungsgemeinschaft (Federal Republic of Germany)
Institut National des Sciences de l'Univers-Centre National de la Recherche Scientifique (France)
Ocean Research Institute of the University of Tokyo (Japan)
National Science Foundation (United States)
Natural Environment Research Council (United Kingdom)
European Science Foundation Consortium for the Ocean Drilling Program (Belgium, Denmark, Finland, Iceland, Italy, The Netherlands, Norway, Portugal, Spain, Sweden, and Switzerland)
Marine High-Technology Bureau of the State Science and Technology Commission of the People's Republic of China

Any opinions, findings, and conclusions or recommendations expressed in this publication are those of the author(s) and do not necessarily reflect the views of the National Science Foundation, the participating agencies, Joint Oceanographic Institutions, Inc., Texas A&M University, or Texas A&M Research Foundation.

The following scientists were aboard the *JOIDES Resolution* for Leg 187 of the Ocean Drilling Program:

David M. Christie
Co-Chief Scientist
College of Oceanic and Atmospheric Sciences
Oregon State University
Oceanography Administration Building 104
Corvallis OR 97331-5503
USA
Internet: dchristie@oce.orst.edu
Work: (541) 737-5205
Fax: (541) 737-2064

Rolf-Birger Pedersen
Co-Chief Scientist
Geologisk Institutt
Universitetet i Bergen
Allégaten 41
Bergen 5007
Norway
Internet: rolf.pedersen@geol.uib.no
Work: (47) 55-58-35-17
Fax: (47) 55-58-94-16

D. Jay Miller
Staff Scientist
Ocean Drilling Program
Texas A&M University
1000 Discovery Drive
College Station TX 77845-9547
USA
Internet: jay_miller@odp.tamu.edu
Work: (979) 845-2197
Fax: (979) 845-0876

Vaughn G. Balzer
Igneous Petrologist
Department of Geosciences
Oregon State University
104 Wilkinson Hall
Corvallis OR 97331-5506
USA
Internet: balzerv@geo.orst.edu
Work: (541) 737-1201
Fax: (541) 737-1200

Florence Einaudi
LDEO Logging Staff Scientist
Laboratoire de Mesures en Forage
ODP/Naturalia et Biologia (NEB)
BP 72
Aix-en-Provence Cedex 4 13545
France
Internet: einaudi@lmf-aix.gulliver.fr
Work: (33) 442-97-1560
Fax: (33) 442-97-1559

M. A. Mary Gee
Igneous Petrologist
Department of Geology
Royal Holloway College
University of London
Egham, Surrey TW20 OEX
United Kingdom
Internet: m.gee@rhbnc.ac.uk
Work: (44) 1784-443-626
Fax: (44) 1784-471-780

Folkmar Hauff
Igneous Petrologist
GEOMAR
Christian-Albrechts-Universität zu Kiel
Department of Volcanology and Petrology
Wischhofstrasse 1-3
Kiel 24148
Federal Republic of Germany
Internet: fhauff@geomar.de
Work: (49) 431-600-2125
Fax: (49) 431-600-2924

Pamela D. Kempton
Igneous Petrologist
Isotope Geosciences Laboratory
Natural Environment Research Council
Kingsley Dunham Centre
Keyworth, Nottingham NG12 5GG
United Kingdom
Internet: p.kempton@nigl.nerc.ac.uk
Work: (44) 115-936-3327
Fax: (44) 115-936-3302

Wen-Tzong Liang
Geophysicist
Institute of Earth Sciences
Academia Sinica
Taipei, Taiwan
P.O. Box 1-55
Nankang
Taipei 11529
Taiwan
Internet: wtl@earth.sinica.edu.tw
Work: (886) 2-2783-9910, ext 508
Fax: (886) 2-2783-9871

Kristine Lysnes
Microbiologist
Institute for Microbiology
University of Bergen
Bergen 5007
Norway
Internet: kristine.lysnes@im.uib.no
Work: 55-58-81-98
Fax: 55-58-96-71

Christine M. Meyzen
Igneous Petrologist
Centre de Recherches Pétrographiques et Géochimiques (UPR 9046)
CNRS
15, rue Notre-Dame-Des-Pauvres
BP 20
Vandoeuvre-Les-Nancy 54501
France
Internet: meyzen@crpg.cnrs-nancy.fr
Work: (33) 3-83-59-42-44
Fax: (33) 3-83-59-17-98

Douglas G. Pyle
Igneous Petrologist
College of Oceanic and Atmospheric Sciences
Oregon State University
Oceanography Administration Building 104
Corvallis OR 97331-5503
USA
Internet: pyle@oce.orst.edu
Work: (541) 867-0191
Fax: (541) 737-2064

Christopher J. Russo
Igneous Petrologist
Department of Geosciences
Oregon State University
Wilkinson Hall 104
Corvallis, OR 97331-5506
USA
Internet: russoc@geo.orst.edu
Work: (541) 737-1201
Fax: (541) 737-1200

Hiroshi Sato
Structural Geologist
Ocean Research Institute
University of Tokyo
1-15-1 Minamidai
Nakano
Tokyo 164-8639
Japan
Internet: satohiro@ori.u-tokyo.ac.jp
Work: (81) 3-5351-6447
Fax: (81) 3-5351-6445

Ingunn H. Thorseth
Igneous Petrologist
Geologisk Institutt
Universitetet i Bergen
Allegaten 41
Bergen 5007
Norway
Internet: ingunn.thorseth@geol.uib.no
Work: (47) 5558-3428
Fax: (47) 5558-9416

SCIENTIFIC REPORT

ABSTRACT

Leg 187 undertook to trace the boundary between Indian and Pacific, ocean-scale mantle provinces across 10- to 30-m.y.-old seafloor of the southeast Indian Ocean between Australia and Antarctica. The boundary has been located on young seafloor of the Australian Antarctic Discordance (AAD), where it is sharply defined and migrating to the west at ~40 mm/yr.

The leg was built around a responsive drilling strategy in which real-time shipboard geochemical analyses from one site were frequently used to guide the selection of subsequent sites from a slate of preapproved targets. This strategy proved highly effective, allowing us to maximize our time on site and to focus on sites that could potentially yield the best definition of the boundary configuration. Using Ba and Zr contents of basalt glasses referenced to our database of younger (0–7 Ma) lavas from the AAD and Zone A (east of the AAD), we assigned each of the 23 holes drilled at 13 sites to an Indian, Pacific, or Transitional-Pacific (TP) mantle domain. Three sites encountered lavas from two of the three domains.

From these shipboard identifications of mantle domain, three fundamental observations can be made:

1. No Indian-type mantle occurs east of the regional residual depth anomaly.
2. Pacific and especially TP-type mantle occurs throughout the depth anomaly in the study area.
3. Between ~25 and 14 Ma, Indian and Pacific mantle types alternated in western Zone A on a time scale of a few million years.

These observations lead to the following tentative conclusions which require careful testing as isotopic data become available. A discrete mantle boundary comparable to the present-day boundary in the AAD cannot be mapped through the entire 14- to 28-Ma time interval encompassed by Leg 187 sites, although comparable boundaries have existed for relatively short, discrete time intervals. We surmise that, for the longer term, the eastern limit of the Indian mantle province corresponds closely to the eastern edge of the depth anomaly. Its locus must lie close to the 500-m residual depth contour that tracks south to connect with the known location of the Indian-Pacific boundary on younger seafloor of the AAD. West of this boundary, sporadic occurrences of lavas indicating derivation from TP-type mantle and even Pacific-type mantle are interspersed with the predominant Indian-type mantle. The western limit of Pacific or TP mantle is not well defined by our data, but it is most likely associated with the western boundary of the depth anomaly. The alternation of Indian-type sites with Pacific and TP-type sites in western Zone A on time scales of a few million years can be interpreted in terms of discrete incursions, either of Indian mantle beneath Zone A or, perhaps more likely, of Pacific mantle into the dominantly Indian region of the depth anomaly.

Samples from Leg 187 will undergo extensive geochemical and isotopic analyses to refine the definition of the isotopic boundary and to improve our understanding of the nature and origin of the AAD, the mantle boundary, and the distinctive Indian Ocean mantle province. In addition, a battery of samples collected as quickly as possible under conditions that were as sterile as possible were placed in a variety of media in order to characterize the microbial population of the deep seafloor. Complementary electron microscope studies will seek to characterize fossil and living microbes within samples and mechanisms involved with biodegradation of basaltic glass.

INTRODUCTION

Background

The Indian and Pacific Mantle Isotopic Provinces

Lavas erupted at Indian Ocean spreading centers are isotopically distinct from those of the Pacific Ocean, reflecting a fundamental difference in the composition of the underlying upper mantle. Along the Southeast Indian Ridge (SEIR), the Indian Ocean and Pacific Ocean mantle isotopic provinces are separated by a uniquely sharp boundary. This boundary has been located to within 25 km along the spreading axis of the SEIR within the Australian Antarctic Discordance (AAD) (Klein et al., 1988; Pyle et al., 1992; Christie et al., 1998), and subsequent off-axis dredge sampling has shown that the Pacific mantle has migrated rapidly westward during at least the last 4 m.y. The principal objective of Leg 187 was to delineate this boundary farther off axis, allowing us to infer its history over the last 30 m.y.

The Australian Antarctic Discordance

The AAD (Fig. 1) is a unique region, encompassing one of the deepest (4–5 km) regions of the global mid-oceanic spreading system. Its anomalous depth reflects the presence of unusually cold underlying mantle and, consequently, of thin crust. Despite a uniform, intermediate spreading rate, the SEIR undergoes an abrupt morphologic change across the eastern boundary of the AAD. The region east of the AAD, known as Zone A, is characterized by an axial ridge with smooth off-axis topography (characteristics usually associated with fast-spreading centers), whereas the AAD, also known as Zone B, is characterized by deep axial valleys with rough off-axis topography (characteristics usually associated with slow-spreading centers). Other anomalous characteristics of the AAD include a pattern of relatively short axial segments separated by long transforms with alternating offset directions, unusually thin oceanic crust, chaotic seafloor terrain dominated by listric extensional faulting rather than magmatism, high upper mantle seismic wave velocities, and an intermittent asymmetric spreading history (Weissel and Hayes, 1971, 1974; Forsyth et al., 1987; Marks et al., 1990; Sempéré et al., 1991; Palmer et al., 1993; West et al., 1994; West, 1997; Christie et al., 1998). The morphological and geophysical contrasts across the eastern boundary of the AAD are paralleled by distinct contrasts

in the nature and variability of basaltic lava compositions, reflecting fundamental differences in magma supply because of strong contrasts in the thermal regime of the spreading center.

Mantle Flow and the Isotopic Boundary

The AAD appears to be the locus of converging asthenospheric mantle flows. This is suggested by multiple episodes of ridge propagation from both east and west toward the AAD (Vogt et al., 1984; Cochran et al., 1997; Sempere et al., 1997; Sylvander, 1998; West et al., 1999) and by recent numerical model studies suggesting that significant, convergent, subaxial mantle flow is an inevitable consequence of gradients in axial depth and upper mantle temperature around the AAD (West and Christie, 1997).

Within Segment B5, the easternmost AAD segment, a distinct discontinuity in the Sr, Nd, and Pb isotopic signatures of axial lavas marks the boundary between Indian Ocean and Pacific Ocean mantle provinces (Klein et al., 1988; Pyle et al., 1990, 1992). The boundary is remarkably sharp, although lavas with "transitional" characteristics occur within 50–100 km of the boundary (Fig. 2). Along the axis of the SEIR, the boundary is located within 20–30 km of the ~126°E transform, the western boundary of Segment B5. The boundary has migrated westward across Segment B5 during the last 3–4 m.y. (Pyle et al., 1990, 1992; Lanyon et al., 1995; Christie et al., 1998).

Although the recent history of this uniquely sharp boundary between ocean basin–scale upper mantle isotopic domains has been reasonably well defined by mapping and conventional dredge sampling, its long-term relationship to the remarkable geophysical, morphological, and petrological features of the AAD had not been determined prior to Leg 187. The AAD is a long-lived major tectonic feature. Its defining characteristic is its unusually deep bathymetry, which stretches across the ocean floor from the Australian to the Antarctic continental margins and which may have existed well before continental rifting began ~100 m.y. ago (Veevers, 1982; Mutter et al., 1985). The trend of this depth anomaly forms a shallow west-pointing V-shape, cutting across the major fracture zones that currently define the eastern AAD segments (Figs. 1, 3). This V-shape implies that the depth anomaly has migrated westward at a long-term rate of ~15 mm/yr (Marks et al., 1991), which is much slower than either the recent migration rate of the isotopic boundary or the majority of the known propagating rifts along the SEIR. Further, the relatively rapid northward absolute motion of the SEIR requires that the mantle "source" of the depth anomaly be linear and oriented approximately north-south. Recently, Gurnis et al. (1998) have suggested that the source of this cold linear anomaly lies in a band of subducted material that accumulated before ~100 Ma at the 660-km mantle discontinuity beneath a long-lived western Pacific subduction zone.

History of the Isotopic Boundary

Prior to Leg 187, the locus and history of the isotopic boundary before ~5 Ma were almost completely unknown. Possible long-term relationships between the isotopic boundary and the

morphologically defined AAD could be divided into two distinct classes (schematically illustrated in Fig. 3). Either the recent (0–4 Ma) isotopic boundary migration simply reflects a localized (~100 km) perturbation of a geochemical feature that has been associated with the eastern boundary of the AAD since the basin opened, or the migration is a long-lived phenomenon that only recently brought Pacific mantle beneath the AAD. In the first case, the boundary could be related either to the depth anomaly or to the eastern bounding transform but not, in the long term, to both. The second possibility, that the isotopic boundary only recently arrived beneath the AAD, was first proposed by Alvarez (1982, 1990), who suggested that Pacific mantle began migrating westward when the South Tasman Rise first separated from Antarctica 40–50 m.y. ago. Limited geochemical support for this hypothesis came from the Indian and transitional isotopic signatures of altered ~38- and ~45-Ma basalts dredged to the north and east of the AAD by Lanyon et al. (1995) and from 60- to 69-Ma Deep Sea Drilling Project (DSDP) basalts that were drilled close to Tasmania (Pyle et al., 1992). Unfortunately, neither sample set is definitive. The dredged samples are from sites within the residual depth anomaly and therefore support two of the three possible configurations. The DSDP samples lie far to the east of the depth anomaly but very close to the continental margin. Their apparent Indian affinity is suspect because of the possibility that their mantle source has been contaminated by nearby subcontinental lithosphere. Finally, the fact that the oldest (~7 Ma) off-axis dredge sample from Zone A is of Pacific-type (Christie et al., 1998) constrains possible loci of the Indian-Pacific boundary to intersect the eastern AAD transform north of approximately 47°45′S.

Objectives

Locating the Isotopic Boundary

The principal objective of Leg 187 was to locate the Indian-Pacific mantle isotopic boundary through its expression in the geochemistry of mid-ocean-ridge basalt (MORB) lavas from 8- to 28-Ma seafloor to the north of the AAD. The clearest definition of this boundary can be seen in the Pb isotopic ratios, but it is clear in Nd and Sr isotopic ratios as well (Fig. 2). Although there are also clear overall differences in the major and trace element compositions between the lava populations of the two provinces, there are few elements that can be relied on to accurately determine the affinity of most individual lavas. Two elemental plots that can reliably assign >90% of our current collection of young lavas are Ba vs. Zr/Ba and MgO vs. Na_2O/TiO_2. These elements were reliably measured by inductively coupled plasma-atomic emission spectroscopy (ICP-AES) aboard the *JOIDES Resolution* throughout the leg. Ba and Zr appear to have enabled us to discriminate between basalts of Pacific affinity and their Indian and transitional counterparts, but Na_2O/TiO_2 did not prove useful for this purpose.

Beyond the Isotopic Boundary

Defining the off-axis configuration and migration history of the Indian/Pacific mantle isotopic boundary is not simply an end in itself. In addition to its interest as a mantle dynamics phenomenon, an improved understanding of this boundary is important for a broader general understanding of the oceanic mantle. In investigating the nature and origins of the AAD, the isotopic boundary and the mantle provinces that it separates, we are also investigating the importance of variations in geochemistry, isotopic composition, temperature, and other physical characteristics of the oceanic upper mantle in a setting where other tectonic variables are relatively constant. Improved knowledge of the distribution of these chemical and physical characteristics in space and time will lead to a better understanding of the dynamics of the oceanic mantle and of its interaction with the magmatic processes of the mid-ocean-ridge system.

Subsurface Biosphere

Recent findings have extended the biosphere to include microbial life in deep subsurface volcanic regions of the ocean floor, and much attention has been focused on the nature of microbes that live on, and contribute to the alteration of, basaltic glass in oceanic lavas (Thorseth et al., 1995; Furnes et al., 1996; Fisk et al., 1998; Torsvik et al., 1998). The first evidence for this phenomenon was from textures in basaltic glass from Iceland (Thorseth et al., 1992). Similar textures were later found in basaltic glass from Ocean Drilling Program (ODP) Hole 896A at the Costa Rica Rift, and the microbial contribution to the alteration history was supported by the presence of DNA along the assumed biogenic alteration fronts (Thorseth et al., 1995; Furnes et al., 1996; Giovannoni et al., 1996). Microbes have recently been documented to inhabit internal fracture surfaces of basaltic glass that specifically were sampled for microbiological studies during *Mir* submersible dives to the Knipovich Ridge (Thorseth et al., 1999). Dissolution textures directly beneath and manganese and iron precipitates adjacent to many individual microbes suggest that microbial activity plays an active role in the low-temperature alteration of ocean-floor basalts.

Sterile rock and sediment samples collected during Leg 187 for microbial culturing, DNA analysis, and electron microscopic study range in age from 14 to 30 Ma, providing an opportunity to study temporal changes in microbial alteration.

Drilling Strategy

In order to fulfill the primary objective of the leg (the location and characterization of the Indian-Pacific mantle isotopic boundary), our drilling strategy was focused on maximizing the number of sites rather than recovery or penetration at any one site. Although our goal for each site was ~50 m penetration into basaltic basement, this was achieved only at five sites. At most sites, drilling conditions were poor as we penetrated broken pillow flows and talus or other rubble; many holes were abandoned when they became unstable.

Much of the region is devoid of measurable sediment cover. Most sites were located on localized sediment pockets detected by single-channel seismic imaging during the *Melville*'s site survey cruises Boomerang 5 (BMRG05) and Sojourn 5 (SJRN05). Three additional sites were surveyed during the transit from Site 1158 to 1159, and two were subsequently drilled as Sites 1161 and 1162. Based on the seismic records, all sites were ranked on a scale of 1 to 3, depending on the clarity with which they were imaged and the width and depth of sediment cover. At highly ranked sites, sediment thickness predictions from site survey data proved to be reasonably accurate, so, whenever possible, we chose higher ranked sites. At Site 1152, only a few meters of soft sediment were encountered, and spud-in conditions were little better than those for bare rock. Two other low-ranked sites, AAD-2B and -3A (Sites 1159 and 1163), proved to have more than adequate sediment cover and were drilled successfully.

As the *JOIDES Resolution* approached each site, we ran a short survey using the 3.5-kHz precision depth recorder (PDR) and, in all but a few cases, the single-channel seismic system to confirm the location and suitability of the proposed site. When possible, these surveys were run obliquely to the original north-south survey lines, but in some cases weather conditions dictated that we run close to the original course. For several smaller sites we chose to run north-south lines to minimize out-of-plane reflections from the dominantly east-west trending topography.

Because sediments across the region were expected to be reworked and possibly winnowed and because basement penetration at as many sites as possible was the primary objective of this leg, we chose in most cases to wash through the sediment section. Wash cores containing significant sediment intervals were recovered at 10 sites.

During Leg 187 we used a responsive drilling strategy. At key points during the leg, subsequent sites were chosen from among the 19 preapproved sites according to the results of onboard geochemical analyses of the recovered basalts.

IGNEOUS PETROLOGY

Introduction

During Leg 187 we drilled 617 m of volcanic basement, recovering 137 m of core. By far the dominant lithology recovered was pillow basalt, either as pillow flows or as basaltic rubble. Also common were basaltic breccias cemented by various types of sedimentary infill, including carbonates, clays and lithic debris. Massive basalts were interlayered with pillow flows at one site (Site 1160). Hole 1162A is also anomalous, as greenschist facies metadiabase, metagabbro and cataclasite were recovered as clasts in a lithic, dolomite-cemented breccia, suggesting that a dike complex has been uplifted and eroded. With the exception of Site 1162, all other holes sampled only the uppermost volcanic carapace, but virtually all the recovered basalts have been pervasively altered, with Fe oxyhydroxide and clay as the typical alteration products. At all but two sites, we washed through 100–200 m of sediment, recovering at most a few meters in wash

barrels. Both clay- and carbonate-rich sediments were encountered. Lithified sediments are present just above the volcanic basement in some holes, with highly varying amounts recovered. The rock types recovered during Leg 187 are summarized in Table 1, and brief descriptions of the typical lithologies are given below.

Pillow Basalt and Basaltic Rubble

Pillow basalts were sampled in all cores either as intact pillow lava or as rubble. Pillows are recognized in the core by their curved chilled margins (Fig. 4), radial fracture patterns, and V-shaped piece outlines. Chilled margins are abundant in most cores, and more than 90 glassy margins were sampled by the science party for postcruise studies. Typically, chilled margins are composed of an outer, 1- to 10-mm, glassy rind that grades through a discrete variolitic zone into a coalesced variolitic zone. Such zones are commonly easily visible in hand specimen as the mesostasis has been turned light brown by alteration, highlighting the variolitic texture. Many of the glassy rinds have attached veneers or crosscutting veins of interpillow sediment that is carbonate rich in some cases and clay rich in others.

Basaltic rubble was recovered from 10 of 23 holes. The rubble is distinguished by multiple weathered surfaces that were not cut by the drill and semirounded forms. Usually, the rubble can be recognized as pillow basalt based on the criteria outlined above. In many holes rubble was encountered just below the contact between sediment and basalt, providing very poor drilling conditions and requiring that the initial hole be abandoned in 9 out of 13 sites. In those instances a second hole was started within 200 m; in all but one case (Site 1158), this second hole allowed us to satisfactorily complete our drilling objectives. In a few holes rubble was encountered at a deeper level, below intact lava flows, demonstrating that at least some of the rubble deposits formed within the active volcanic zone.

Massive Basalt

Massive basalts, with recovered (and, hence, minimum) thicknesses of as much as 1.5 m were recovered only from Hole 1160B. These can be distinguished by long (up to 50–60 cm), continuous core pieces with uniform texture (Fig. 5). In Hole 1160B each of the three massive basalts is overlain by a pillow flow of similar lithology. In one massive flow, olivine phenocrysts increase in abundance toward the base, suggesting that there has been some crystal settling. No chilled margins were recovered from the massive units. Site 1160 is the easternmost of the Leg 187 drilled sites. It is located at the northern foot of a 1500-m-high seamount in the middle of Zone A. The abundance of massive flows at this site may reflect the generally robust magmatism of the SEIR, or it may reflect increased magmatism related to the seamount itself.

Interpillow Sediments and Basaltic Breccias

Basalts are intimately associated with sediments at 8 of the 13 sites. Sediment may be present as interpillow fill, as fracture fill, and as both small clasts and matrix material in breccias of

various types. Interpillow and fracture fills are common in Holes 1155B and 1163A, where micritic limestone is attached to infills fractures in the glassy margins (Fig. 6). The fracture infills extend deep into individual pieces, and they are typically made up of micritic sediment containing sand-sized or smaller glass/palagonite and basalt fragments. Subsequent diagenetic and wall-rock reactions, probably related to fluid flow through the fractures, have transformed the simple fracture fill to a composite, partly sedimentary, partly hydrothermal vein fill.

The breccias can be subdivided into (1) volcanic breccias, formed during or soon after eruption, and (2) breccias that formed after extensive basalt alteration. The best examples of volcanic breccia are found in Holes 1159A, 1163A, and 1164A. Hyaloclastite breccia, consisting of angular to subrounded glass/palagonite in a clay matrix, was recovered from Hole 1159A, and hyaloclastite breccia with calcarenitic to calcareous clayey matrix is present in Hole 1163A. Rounded glass fragments included in the carbonate matrix suggest that some of the lava flows sampled in Hole 1159A erupted onto a sedimented surface. Volcanic breccia dominated by aphyric basalt and glass/palagonite clasts was sampled in Hole 1164A. This breccia differs from all other Leg 187 breccias in having only insignificant amounts of nonlithic sedimentary matrix.

Posteruptive, carbonate-cemented breccias are prominent in seven holes (Holes 1155B, 1156A, 1157A, 1161A, 1161B, 1162A, and 1162B). The multistage, posteruptive evolution of these breccias is evident in the common truncation by fracturing of distinct alteration halos around the original clast margins and in the common occurrence of composite sediment-basalt clasts. Breccias of this type range from matrix supported (Fig. 7) to clast supported, with clast sizes varying from several tens of centimeters to a few millimeters. The carbonate-cemented basalt breccia from Hole 1156A has a particularly complex history: much of the clast material has a multistage alteration and fracturing history, and there are two generations of matrix carbonate (Fig. 8) followed by late-stage carbonate veining. The formation of this breccia must have involved deposition and redeposition of talus in a tectonically active setting, accompanied and followed by sediment deposition, lithification, and, ultimately, carbonate veining.

Dolomite-cemented basalt breccias were recovered from Holes 1162A and 1162B. In Hole 1162A, a polymict clast assemblage composed of greenschist facies metagabbro, metadiabase, basalt, and cataclasites is cemented by crystalline dolomite with a subsidiary fine lithic component that imparts variable bright red and green colors to the matrix. All the clasts in Hole 1162B are very highly altered basalts that have been transformed almost entirely to clay under low-temperature conditions.

Petrography of Basalts

Leg 187 basalts range from aphyric (Fig. 9) to moderately phyric (Fig. 10), with small vesicles, up to 1–2 mm in size, in a small proportion of the rocks. Plagioclase and olivine are the typical phenocryst phases, with plagioclase being most abundant. No systematic spatial or temporal variations in the abundances of phenocryst phases were observed. Cr spinel is present in accessory amounts as small, euhedral inclusions in plagioclase and olivine phenocrysts or as

discrete subhedral crystals up to 0.5 mm in size. Clinopyroxene phenocrysts and microphenocrysts are present only in Holes 1152B and 1164A. These holes are located in Segments B4 and B5 near the western margin of the depth anomaly. At the spreading axis, these zones are characterized by relatively unevolved lavas with a high degree of compositional variability for a given MgO content. These characteristics suggest an array of primary magma compositions, with minimal mixing and differentiation at crustal levels. The presence of clinopyroxene phenocrysts at these sites, in lavas of relatively high MgO content, may reflect high-pressure fractionation within these more magma-starved segments.

As many as 30% of the phenocrysts are glomerocrysts. These range from centimeter-sized loose clusters of prismatic plagioclase and equant olivine (Fig. 11) to tightly intergrown aggregates. Corroded xenocrysts and xenocrystic aggregates (Fig. 12) are present in several samples from different cores; disequilibrium textures, including discontinuous zoning and sieve-textures (Fig. 13), are common in the larger plagioclase phenocrysts.

Groundmass textures in the pillow basalts are typically microcrystalline, ranging from intersertal to sheaf quench crystal morphologies. Groundmass is usually dominated by acicular to skeletal plagioclase, with equant, often skeletal, olivine forming in subordinate amounts. Clinopyroxene occurs predominantly as plumose quench growths (Fig. 14) or as bundles of bladed crystals, but larger, anhedral to euhedral, granular to prismatic, crystals occur adjacent to and within miarolitic cavities in several holes. The massive flows in Hole 1160B show intergranular to subophitic groundmass textures (Fig. 15).

ALTERATION

Basalts recovered during Leg 187 have all been subjected to low-temperature alteration. Macroscopically, alteration is manifested most commonly as (1) alteration halos around the margins of pieces and (2) following veins and open fractures. There is a broad range of alteration intensity within and between sites, from completely fresh, to incipient iron staining, to pervasive discoloration. Alteration phases replacing phenocrysts and groundmass include abundant Fe oxyhydroxides and clay minerals, with common cryptocrystalline silica and Mn oxide encrustations. Less commonly, carbonate has replaced groundmass and precipitated along veins. At one site, greenschist facies assemblages were recovered.

Low-Temperature Alteration

Phenocrysts and Groundmass

Distinctive concentric low-temperature alteration halos commonly follow the shapes of the outer surfaces of individual basalt pieces. On cut surfaces, these halos mimic the extent of red-brown alteration on exterior facets of pieces that show no evidence of drilling abrasion, suggesting that many of the pieces recovered were basaltic rubble accumulated in the valleys that

we, of necessity, selected as drilling targets. However, at several sites, we recovered drill-cut, contiguous pieces showing the normal progression from palagonitized glassy margins, through altered zones of discrete and/or coalesced spherulites, to holocrystalline basalt (Figs. 16, 17), indicating that intact pillows were sampled.

Alteration halos on core pieces usually have sharp, smooth contacts with the less altered piece interiors (Fig. 18), although some are gradational and/or irregular. At most sites, several zones can be distinguished in these alteration rinds, progressing from more intensely altered rims where Fe oxyhydroxides and clay pervasively replace groundmass and phenocrysts alike, to less intensely altered areas where only groundmass phases are altered.

In at least some pieces from every site, low-temperature alteration is pervasive. This alteration is developed as brown-red discoloration of the entire piece, apparent on drill-cut exteriors of pieces as well as on the cut faces of cores. In these pieces the groundmass and most phenocrysts are altered to Fe oxyhydroxide and clay, although fresh kernels are common. In both alteration halos and pervasively altered pieces, olivine phenocrysts are much more intensely altered than plagioclase. Fe oxyhydroxide and clays commonly only highlight cleavage planes, fractures, and crystal margins in plagioclase.

The most widespread evidence of low-temperature alteration seen in thin section is partial to complete replacement of quench textured phases and mesostasis by Fe oxyhydroxide and clay (Fig. 19). Crystalline groundmass phases are variably altered through replacement of olivine, clinopyroxene, and mesostasis to smectite and Fe oxyhydroxide, visible as a pervasive or patchy discoloration and cloudy appearance. Groundmass plagioclase is usually fresh or incipiently altered.

Olivine phenocrysts are commonly completely altered, or nearly so, to clay, Fe oxyhydroxide, and magnetite. In some sections, olivine pseudomorphs show euhedral grain shapes, but only the cores of grains are preserved. In others, olivine alteration is restricted to fractures. The main alteration product of plagioclase is Fe oxyhydroxide, mostly along cleavage planes and fractures. Plagioclase is rarely completely replaced; in nearly every thin section there is more fresh than altered plagioclase.

Overall alteration characteristics vary from site to site. Sites 1152, 1153, and 1154 are only slightly altered. This is interesting in that these are the oldest sites we drilled (~26 to 28 Ma). Alteration at these sites is expressed as only minor replacement of groundmass and phenocrysts by secondary phases. Sites 1161 and 1162, associated with a westward propagating rift, are predominantly carbonate- and/or silica-cemented breccias, and both show moderate to high degrees of alteration. Angular basalts clasts in the breccia are commonly pervasively altered, and at least some of the alteration occurred prior to brecciation, as evidenced by matrix cutting through alteration halos. Site 1164, our last site, shows the most pervasive effects of alteration and was interpreted to have sampled only basaltic rubble (see “Igneous Petrology”). All other sites showed a range of slight to moderate alteration, less intense overall than Sites 1161, 1162,

and 1164, although we recovered at least a few pieces of pervasively altered basalt at every site. The effects of alteration on bulk rock composition are discussed in "Geochemistry."

Glass

Palagonitized pillow rinds ranging in thickness from 0.5 to 10 mm were sampled at every site. Within the rinds, fresh, black, basaltic glass is common, but there is ubiquitous yellow to orange palagonite with dull surfaces in places crosscut by a dense network of anastomosing silica (Fig. 20) and, more rarely, silica and calcite veins. These veins are most commonly oriented subparallel to rind margins, although crosscutting veins are also abundant. Fresh glass and palagonite commonly occur in thin (0.5–2 mm), irregularly interlayered sheets, with palagonite being most abundant (>90%) in the outermost sections. In thin section, altered glass rims show weak parallel banding, except at the alteration front, which often displays dendritic features extending into fresh glass and believed to be related to microbial degradation (Thorseth, et al., 1995) (Fig. 21).

Veins

Veins are present in all the cores. They include both compositionally homogeneous and composite veins, as well as rare crack-seal veins. Veins filled with combinations of silica, Fe oxyhydroxide, clay, and Mn oxide are present at every site, whereas calcite-bearing veins were only observed at Sites 1153, 1155, 1156, 1157, 1160, and 1163. The most common vein assemblage where carbonate was observed includes thin (<1 mm) linings of cryptocrystalline silica along vein selvages, spotted with sporadic submillimeter Mn oxide accompanied by fillings of microcrystalline to cryptocrystalline calcite (Fig. 22). Additionally at these sites, it is not unusual to see composite veins that change from silica filling within the palagonitized glass and chilled margins to calcite filling toward the interiors of pillow fragments. Sites 1160 and 1162 were unique in that these were the only sites where chlorite is a common vein-filling phase. Dolomite veins are present only in cores from Site 1162. Sediment-filled fractures are common in breccia clasts and pillow lavas that retain adhered interpillow sediment. At Site 1156, sediment-filled fractures and the breccia matrix contain two generations of calcite. First, a drusy pink micritic calcite permeates the sediment and breccia matrix; subsequently, sparry calcite precipitated along fractures and in void spaces.

Greenschist Facies Metamorphism

At Site 1162, a number of breccia clasts have developed a distinct greenschist facies alteration mineralogy. Macroscopically, both aphyric and phyric basalts are greenish brown, strikingly different in color to any other rocks recovered during Leg 187. Olivine phenocrysts are completely replaced by Fe oxyhydroxide and a pale yellow combination of chlorite, talc, and clay. Groundmass olivine and clinopyroxene are extensively replaced by Fe oxyhydroxide and

clay in most pieces, and several pieces have a chloritized groundmass. The presence of chlorite indicates that these rocks underwent metamorphism at 150°–250°C (Alt et al., 1996).

Somewhat more intense high-temperature alteration has affected gabbro and diabase breccia clasts recovered at this site. Fibrous actinolite and chlorite replace clinopyroxene, and olivine is totally replaced by concentric layers of talc, chlorite, and magnetite. Plagioclase is partially replaced by clay and chlorite and is recrystallized to albite along grain margins. Thin veins (<1 mm) are filled with chlorite and clay. The occurrence of actinolite, talc, chlorite, and albite in upper crustal basalts is consistent with lower greenschist facies metamorphism (Alt et al., 1996).

GEOCHEMISTRY

Introduction

The rapid-turnaround shipboard analytical capability provided by the new ICP-AES instrument was fundamental to the success of Leg 187. At several points throughout the leg, data from one site were used in deciding which of two or even three alternate plans would be followed for the succeeding few sites. This reactive strategy enabled us to rapidly determine that the isotopic boundary is closely related to the eastern side of the regional depth anomaly. We were then able to focus with confidence on sites in the vicinity of the depth anomaly, to the exclusion of sites in eastern Zone A.

The Indian-Pacific mantle boundary was originally identified within the AAD on the basis of isotopic ratios in seafloor lavas, and these ratios, particularly $^{206}Pb/^{204}Pb$, continue to be the only definitive discriminants between Pacific and Indian mantle provinces (Fig. 23). In planning for Leg 187, we worked exhaustively with our data from zero-age and young (<7 Ma) dredge samples throughout the AAD and Zone A to identify a reliable discriminant that could be analyzed onboard the *JOIDES Resolution*. A single element, barium, appeared to be both reliable as a discriminant and relatively easy to determine with the necessary accuracy. For ease of use, we settled upon a single diagram, Zr/Ba vs. Ba, as providing a clear, visual discrimination between Indian-type and Pacific-type lavas from our 0- to 7-Ma data set. A second element ratio, Na/Ti (expressed as Na_2O/TiO_2 throughout this report), also appeared to have potential as a discriminant, although both elements are susceptible to fractionation by a variety of magmatic processes. As it turned out, the 0- to 7-Ma dividing line on this diagram does not apply to most Leg 187 sites, so we relied almost exclusively on Ba-Zr systematics in our decision-making process. Nevertheless, the Ba-Zr systematics that we are relying on are an imperfect discriminant, which means that later isotopic analysis may lead to definitive assignment of some sites that are currently classified as transitional. It is also possible, though less likely, that some sites are currently misidentified and may be reassigned when the isotope data become available.

The glasses from Leg 187 sites are all relatively primitive in composition, with MgO ranging from 9.4 to 7.2 wt%. With few exceptions, whole-rock samples have significantly lower MgO contents than the associated glasses. In the most extreme cases, whole-rock MgO values are

lower by >3.0 wt%; in most cases these are lower by 0.5–1.0 wt%. Variations in MgO are seldom accompanied by coherent variations in other elements and, therefore, cannot be attributed to crystallization or other magmatic processes. A particularly clear example of this phenomenon is provided by Hole 1160B, which recovered seven lithologic units, three of which are massive flows interspersed with pillow flows. Each massive flow is overlain by a pillow flow of the same lithology. Whole-rock samples from all three massive flows and glasses from two of the overlying pillow flows are essentially identical in composition with ~8.9–9.1 wt% MgO (Fig. 24). Whole rocks from the pillow flows, however, have lower MgO contents, differing from the glasses by as much as 3–4 wt% MgO. Most other elements in the pillow whole rocks are similar in abundance to the glasses and massive flows. We conclude from these observations that MgO is selectively removed from pillow interiors as a result of the pervasive low-temperature alteration that has affected all our sites.

The data for elements not discussed above have received only cursory examination, but apparently there has been significant temporal variation in primary magma compositions in all three segments. For Segments B4 and B5, these variations are likely related to the westward migration of the depth anomaly relative to the segment boundaries. In Zone A, temporal variability appears to have been modulated by repeated rift propagation.

Mantle Domain Recognition

Barium and Zirconium

Throughout Leg 187, we used ICP-AES Ba and Zr data to determine mantle domain based on the 0- to 7-Ma data fields in the Zr/Ba vs. Ba diagram. Because of the potential for alteration of Ba content by seawater alteration, we used only hand-picked basalt glasses in making this determination. Figure 25 shows all available glass data from the AAD region. There is a clear dividing line between glasses from the Indian mantle domain and those from the Pacific domain. A tie line connecting all the glasses from the transitional domain beneath Segment B5 cuts across both fields. The only 0- to 7-Ma lavas that do not fall within the clearly defined Indian and Pacific fields are a small group of primitive lavas from propagating rift tips in Zone A.

Leg 187 glass data are plotted in relation to the 0- to 7-Ma Ba-Zr fields and the B5 tie line in Figure 26A. Although many of the Leg 187 data plot within or very close to the 0- to 7-Ma fields and can readily be assigned to one of the 0- to 7-Ma fields, there is an important group of data that cannot. These data plot in the area below the Pacific field (i.e., toward lower Zr/Ba and slightly higher Ba than the majority of Pacific-type lavas). We refer to these lavas as Transitional-Pacific (TP) type because they appear to represent an extension of the Pacific field toward the compositions of the Zone A propagating rift tip lavas (Fig. 26A). This extension may reflect a temporal shift in any of several source parameters, including source composition and overall extent of melting or a shift in the mixing proportions of one or more mantle end-member components. It could also reflect some form of addition of Ba to the samples from seawater, either directly by low-temperature alteration or indirectly by assimilation of altered crust into the

magma. In terms of the Zr/Ba vs. Ba diagram, basaltic liquids plotting in the TP field could also have been derived, by normal crystal fractionation processes, from Indian-type parents. Such processes would be expected to produce trends that cut across the observed data array at a high angle. Cursory examination of the data does not, however, support a fractionation origin for the TP glasses, as there is no apparent progression to decreasing MgO across the Indian field or into the TP field. Finally, the TP field is distinct from the B5 tie line and is therefore unlikely to reflect mixing between Indian and Pacific domains.

Sodium and Titanium

For the 0- to 7-Ma glasses, a plot of Na_2O/TiO_2 vs. MgO effectively discriminates Indian domain glasses from those of the Pacific domain, again with the B5 tie line crossing the divide between domains (see Fig. 25B). Unfortunately, this diagram does not apply in a straightforward way to the Leg 187 glasses. In Figure 26B, Leg 187 glass data are plotted on this diagram and coded as Indian, Pacific or Transitional Pacific, according to their position on the Zr/Ba vs. Ba diagram (Fig. 26A). According to this division, no Leg 187 Indian-type lava plots in the 0- to 7-Ma "Indian" field, and lavas of all three types are intermixed in the "Pacific" field.

Although it is offset to lower Na_2O/TiO_2 than the 0- to 7-Ma field, Leg 187 Indian lavas do define a discrete field, although this field also encompasses several TP and Pacific lavas. The three Pacific lavas are, however, all from Site 1160; these also have the three lowest Ba contents of the Leg 17 Pacific lavas. In Figure 26A, they plot to the left of the B5 tie line. The only other sample with comparable low Ba is the borderline Pacific sample from Site 1164 that is plotted as a red triangle in the figure.

The offset of the Pacific and Indian fields appears to reflect the generally low Na_2O contents of Leg 187 glasses relative to those of the AAD. Whether this apparently fundamental shift in primary magma chemistry reflects a temporal change in mantle temperature and/or extent of melting, a change in the source composition or some other source parameter cannot be readily evaluated without further data.

Distribution of Mantle Domains

Most of the Leg 187 sites are distributed along three north-south transects, one each in Segments B4 and B5 and one in western Zone A (Figs. 27, 28). There are two additional sites in eastern Zone A.

Segments B4 and B5

Indian-type mantle was present beneath all three B5 sites and one B4 site (Site 1163) at their time of eruption. At two sites, basalts derived from two distinct mantle types were erupted in close proximity. Glasses from Hole 1155A are of TP type, whereas those from Hole 1155B, 200 m away, are of Indian type. Glasses from Holes 1164A and 1164B are of Pacific and Indian types, respectively, although the Pacific glass plots very close to the boundary between the two

fields. (This glass is represented by a red triangle in Fig. 26A.) Only TP-type glass was recovered at Site 1152.

Zone A West

Six sites form a transect between crustal ages 28–14 Ma in western Zone A (Figs. 27, 28). Along this transect, Indian-type mantle was present at ~25 and 14 Ma, but in three out of four cases the transition between Indian- and Pacific-type is constrained to have taken place at no more than 2–3 Ma. (The fourth transition, north of Site 1157, is not constrained as there is no site in this area.)

Zone A East

Sites 1154 and 1160 in eastern Zone A are distinctly of Pacific character (Figs. 27, 28).

Summary

Taking the shipboard identifications of mantle domain at face value, three fundamental observations can be made:

1. No Indian-type mantle occurs east of the 500-m contour on the regional depth anomaly. At ~6 Ma, this contour is very close to the rough-smooth terrain boundary that marks the isotopic boundary in Segment B5.
2. Pacific- and especially TP-type mantle occurs throughout the region of the depth anomaly, at least in the older part of the study area.
3. Between ~25 and 14 Ma, Indian and Pacific mantle types alternated in western Zone A on a time scale of a few millions of years, comparable to the time scale of the recent migration of the Pacific mantle across Segment B5.

From these observations we draw the following tentative conclusions. These conclusions are not unique, however, and they will require careful testing as the isotopic data become available.

A discrete mantle boundary comparable to the present-day boundary in the AAD cannot be mapped through the entire 14- to 28-Ma time interval encompassed by Leg 187, although comparable boundaries may have existed for relatively short, discrete time intervals. For the longer term, it appears likely that the eastern limit of the Indian-mantle province corresponds closely to the eastern edge of the depth anomaly. The locus of this boundary is unconstrained, but it must lie close to the 500-m residual depth contour. West of this boundary, and perhaps coinciding with the >500-m region of the depth anomaly, Indian mantle predominates, but occurrences of Transitional-Pacific- and even Pacific-type mantle are not uncommon. The western limit of Pacific or TP mantle is not well defined by our data, but it cannot be farther east than the 400-m residual depth contour.

The alternation of Indian-type sites with Pacific- and TP-type sites along the western Zone A transect from 14 to 25 Ma suggests a rapid alternation of discrete mantle types on time scales of a few million years, comparable to that of the current migration in the AAD. These occurrences can be interpreted as discrete incursions, either of Indian mantle beneath Zone A or, equally plausibly, of Pacific mantle into the dominantly Indian region of the depth anomaly. If either interpretation is correct, then a discrete Indian-Pacific boundary likely existed for much of that time.

TP-type mantle is not represented in our 0- to 7-Ma data set, but it appears to be an extension of the Pacific-mantle field, rather than a transition between Pacific and Indian types. This type may manifest a mantle component that cannot be seen in the well-mixed, high-flux magma systems of Zone A. In the region of the depth anomaly, magma flux is greatly reduced and small magma batches with a variety of individual source signatures may be erupted without severe modification.

CONCLUSION

By any measure, Leg 187 was highly successful. We recovered samples from 23 holes at 13 sites with an average water depth of almost 5 km. In the process, a record 140 km of drill string was passed through the drill floor. In part, this success relates to the unusually mild weather that we encountered. In larger part, it relates to the extraordinary dedication of the *JOIDES Resolution* and ODP crews. Our reactive drilling strategy worked well. After very limited teething troubles with sample preparation and running of the new ICP-AES instrument, we were able to obtain the geochemical data that we needed within 12 hr of “core on deck” for critical samples.

Our principal objective was to determine the configuration of the Indian-Pacific mantle isotopic boundary beneath 10- to 30-Ma seafloor north of the AAD. Using the shipboard Ba and Zr data, we have tentatively outlined the boundary, but definitive answers (and the fulfillment of our objective) will require onshore isotopic analyses. The discrete isotopic boundary that has migrated across Segment B5 of the AAD over the last 3–4 m.y. is probably not a permanent feature, but we believe that we have identified two similar migration events in western Zone A at about 19 and 22 Ma. Over the long term, the Indian-Pacific boundary is probably represented by a transitional region that coincides with the regional depth anomaly. This region appears to be dominated by Indian-type mantle with common, discrete occurrences of TP- and even Pacific-type mantle. In western Zone A, along the eastern boundary of the depth anomaly, Pacific- and Indian-type mantle domains appear to alternate on a time and spatial scale that is comparable to the present-day migration in Segment B5. It is unclear whether this alternation represents short-lived incursions of (1) Indian mantle beneath Zone A or (2) Pacific mantle into the depth anomaly. By analogy with the present day and because Pacific mantle is most commonly

associated with robust magmatism, the latter seems more likely.

Samples from Leg 187 will undergo extensive geochemical and isotopic analysis onshore. Initially, these studies will serve to confirm the mantle provenance of the lavas that we sampled and refine or understanding of the location and nature of the mantle isotopic boundary. Further study will allow us to better understand changes in mantle composition, temperature, dynamics, melting conditions, and magma evolution. Comparative studies with other regions worldwide will enable us to improve our understanding of the nature of both mantle domains and of the origin and evolution of the depth anomaly and the AAD.

Although results will not be available for some time, the microbiology objectives of the leg have been well served. Between two and six samples were taken at each site. The samples include a range of lithologies, including pillow rims, pillow interiors, massive flows, and various breccias. The samples also vary in the extent and type of alteration. Samples will be cultured in a variety of media, at low and high pressures. Electron microscope studies will attempt to characterize living and fossil microbes within samples.

REFERENCES

Alt, J.C., Laverne, C., Vanko, D.A., Tartarotti, P., Teagle, D.A.H., Bach, W., Zuleger, E., Erzinger, J., Honnorez, J., Pezard, P.A., Becker, K., Salisbury, M.H., and Wilkens, R.H., 1996. Hydrothermal alteration of a section of upper oceanic crust in the eastern equatorial Pacific: a synthesis of results from Site 504 (DSDP Legs 69, 70, and 83, and ODP Legs 111, 137, 140, and 148.) *In* Alt, J.C., Kinoshita, H., Stokking, L.B., and Michael, P.J. (Eds.), *Proc. ODP, Sci. Results,* 148: College Station, TX (Ocean Drilling Program), 417–434.

Alvarez, W., 1982. Geological evidence for the geographical pattern of mantle return flow and the driving mechanism of plate tectonics. *J. Geophys. Res.,* 87:6697–6710.

————, 1990. Geologic evidence for the plate driving mechanism: the continental undertow hypothesis and the Australian-Antarctic Discordance. *Tectonics,* 9:1213–1220.

Cande, S.C., LaBrecque, J.L., Larson, R.L., Pitmann, W.C., III, Golovchenko, X., and Haxby, W.F., 1989. Magnetic lineations of the world's ocean basins. *AAPG Map Ser.,* 131.

Christie, D.M., West, B.P., Pyle, D.G., and Hanan, B., 1998. Chaotic topography, mantle flow and mantle migration in the Australian-Antarctic Discordance: *Nature,* 394:637–644.

Cochran, J.R., and Sempéré, J.-C., 1997. The Southeast Indian Ridge between 88°E and 118°E: gravity anomalies and crustal accretion at intermediate spreading rates. *J. Geophys. Res.,* 102:15463–15487.

Fisk, M.R., Giovannoni, S.J., and Thorseth, I.H., 1998. Alteration of oceanic volcanic glass: textural evidence of microbial activity. *Science,* 281:978–979.

Forsyth, D.W., Ehrenbard, R.L., and Chapin, S., 1987. Anomalous upper mantle beneath the Australian-Antarctic Discordance. *Earth Planet. Sci. Lett.,* 84:471–478.

Furnes, H., Thorseth, I.H., Tumyr, O., Torsvik, T., and Fisk, M.R., 1996. Microbial activity in the alteration of glass from pillow lavas from Hole 896A. *In* Alt, J.C., Kinoshita, H., Stokking, L.B., and Michael, P.J. (Eds.), *Proc. ODP, Sci. Results,* 148: College Station, TX (Ocean Drilling Program), 191–206.

Giovannoni, S.J., Fisk, M.R., Mullins, T.D., and Furnes, H., 1996. Genetic evidence for endolithic microbial life colonizing basaltic glass/seawater interfaces. *In* Alt, J.C., Kinoshita, H., Stokking, L.B., and Michael, P.J. (Eds.), *Proc. ODP, Sci. Results,* 148: College Station, TX (Ocean Drilling Program), 207–214.

Gurnis, M., Muller, R.D., and Moresi, L., 1998. Cretaceous vertical motion of Australia and the Australian-Antarctic Discordance. *Science,* 279:1499–1504.

Klein, E.M., Langmuir, C.H., Zindler, A., Staudigel, H., and Hamelin, B., 1988. Isotope evidence of a mantle convection boundary at the Australian-Antarctic Discordance. *Nature,* 333:623–629.

Lanyon, R., Crawford, A.J., and Eggins, S., 1995. Westward migration of Pacific Ocean upper mantle into the Southern Ocean region between Australia and Antarctica. *Geology,* 23:511–514.

Marks, K.M., Vogt, P.R., and Hall, S.A., 1990. Residual depth anomalies and the origin of the Australian-Antarctic Discordance Zone. *J. Geophys. Res.,* 95:17325–17337.

Marks, K.M., Sandwell, D.T., Vogt, P.R., and Hall, S.A., 1991. Mantle downwelling beneath the Australian-Antarctic Discordance Zone: evidence from geoid height versus topography. *Earth Planet. Sci. Lett.,* 103:325–338.

Mutter, J.C., Hegarty, K.A., Cande, S.C., and Weissel, S.C., 1985. Breakup between Australia and Antarctica: a brief review in the light of new data. *Tectonophysics,* 114:255–279.

Palmer, J., Sempéré, J.-C., Christie, D.M., and Phipps-Morgan, J., 1993. Morphology and tectonic of the Australian-Antarctic Discordance between 123° E and 128° E. *Mar. Geophys. Res.,* 15:121–151.

Pyle, D.G., 1994. Geochemistry of mid-ocean-ridge basalt within and surrounding the Australian Antarctic Discordance. [Ph.D. Dissert.]. Oregon State Univ., Corvallis.

Pyle, D.G., Christie, D.M., and Mahoney, J.J., 1990. Upper mantle flow in the Australian-Antarctic Discordance. *Eos,* 71:1388. (Abstract)

————, 1992. Resolving an isotopic boundary within the Australian-Antarctic Discordance. *Earth Planet. Sci. Lett.,* 112:161–178.

Pyle, D.G., Christie, D.M., Mahoney, J.J., and Duncan, R.A., 1995. Geochemistry and geochronology of ancient southeast Indian and southwest Pacific seafloor. *J. Geophys. Res.*, 100:22261–22282.

Sempéré, J.-C., Cochran, J.R. and others, 1997. The Southeast Indian Ridge between 88° and 118°E: variations in crustal accretion at a constant spreading rate. *J. Geophys. Res.*, 102: 15489–15505.

Sempéré, J.-C., Palmer, J., Phipps-Morgan, J., Christie, D.M., and Shor, A.N., 1991. The Australian-Antarctic Discordance. *Geology*, 19:429–432.

Sylvander, B.A., 1998. The Southeast Indian Ridge: Water contents of MORB glasses and chemical effects of propagating rifts. [M.S. Thesis]. Oregon State Univ., Corvallis.

Thorseth, I.H., Furnes, H., and Heldal, M., 1992. The importance of microbiological activity in the alteration of natural basaltic glass. *Geochim. Cosmochim. Acta*, 56:845–850.

Thorseth, I.H., Pedersen, R.B., Daae, F.L., Torsvik, V., Torsvik, T., and Sundvor, E., 1999. Microbes associated with basaltic glass from the Mid-Atlantic Ridge. Conf. Abstr., 4:254. Cambridge Publications, EUG 10, Strasbourg.

Thorseth, I.H., Torsvik, T., Furnes, H., and Muehlenbachs, K., 1995. Microbes play an important role in the alteration of oceanic crust. *Chem. Geol.*,126:137–146.

Torsvik, T., Furnes, H., Muehlenbachs, K., Thorseth, I.H., and Tumyr, O.,1998. Evidence for microbial activity at the glass-alteration interface in oceanic basalts. *Earth Planet. Sci. Lett.*, 162:165–176.

Veevers, J.J., 1982. Australian-Antarctic depression from the mid-ocean ridge to adjacent continents. *Nature*, 295:315–317.

Vogt, P.R., Cherkis, N.K., and Morgan, G.A., 1984. Project Investigator-1: evolution of the Australian-Antarctic Discordance from a detailed aeromagnetic study. *In* R.L. Oliver, P.R. James, and Jago, J. (Eds.), *Antarctic Earth Science: Proceedings 4th International Symposium on Antarctic Earth Sciences:* Canberra (Aust. Acad. Sci.).

Weissel, J.K., and Hayes, D.E., 1971. Asymmetric seafloor spreading south of Australia. *Nature*, 231:518–522.

————, 1974. The Australian-Antarctic Discordance: new results and implications. *J. Geophys. Res.,* 79:2579–2587.

West, B.P., 1997. Mantle flow and crustal accretion in and near the Australian-Antarctic Discordance. [Ph.D. Thesis]. Univ. of Washington, Seattle.

West, B.P., and Christie, D.M., 1997. Diversion of along-axis asthenospheric flow beneath migrating ridge-transform-ridge intersections. *Trans. Am. Geophys. Union,* 78 (Suppl.):673.

West, B.P., Lin, J., and Christie, D.M., 1999. Forces driving ridge propagation. *J. Geophys. Res.*, 104:22845–22858.

West, B.P., Sempéré, J.-C., Pyle, D.G., Phipps-Morgan, J., and Christie, D.M., 1994. Evidence for variable upper mantle temperature and crustal thickness in and near the Australian-Antarctic Discordance. *Earth Planet. Sci. Lett.,* 128:135–153.

TABLE CAPTION

Table 1. Summary of igneous petrology, Leg 187.

FIGURE CAPTIONS

Figure 1. Regional map of the southeast Indian Ocean (from Pyle et al., 1995) showing magnetic lineations (Cande et al., 1989), the Australian Antarctic Discordance (AAD), and Deep Sea Drilling Program sites that sampled basement. Thin dark V east of the AAD is the inferred trace of the isotopic boundary for a migration rate of ~40 mm/yr. The broader gray V is the approximate trace of the regional depth anomaly. Bull's-eye symbols south of Australia indicate approximate positions of dredges by Lanyon et al. (1995). The darkly outlined box shows area of operations for Leg 187; the lighter outlined box shows area of Figure 3.

Figure 2. Along-axis profiles of isotopic ratios from the Southeast Indian Ridge (SEIR) between 114°E and 138°E. The horizontal scale (in kilometers) is the distance from the eastern bounding transform of the Australian Antarctic discordance (AAD). Open symbols and lightly shaded field = Pacific-type mid-ocean-ridge basalt (MORB). Solid symbols and darker field = Indian-type MORB (from Pyle et al., 1992). Triangles = data from Klein et al. (1988), squares = data from the edge of the AAD, and triangles with included circles = samples from west of the AAD. In the lowermost panel, filled circles = dredge depths and open circles = subsidence curve fits to flanks.

Figure 3. Mantle boundary configurations allowed by pre-Leg 187 geochemical data from the dredge sites shown. Indian and Pacific populations are the same as those in Figure 2. Migration across Segment B5 is confirmed, with the boundary constrained to the vertically ruled area labeled "Migrating boundary in B5." East of the Australian Antarctic Discordance (AAD), a hypothetical boundary produced by long-term westward migration is constrained to the medium-gray shaded region in the upper right quadrant. Alternate boundary configurations are associated with the curving trace of the depth anomaly or oscillation between the easternmost AAD transforms. The more southerly Leg 187 drill sites are shown as dark gray solid circles. The remaining sites lie to the north and east of this map. Magnetic anomalies are numbered 2–5. SEIR = Southeast Indian Ridge.

Figure 4. Pillow fragment with chilled margin and distinctive V-shaped, fracture-induced morphology (interval 187-1164B-8R-1, 23–27 cm).

Figure 5. Close-up photograph of interval 187-1160B-4R-2, 54–70 cm, a fresh continuous core of massive basalt.

Figure 6. Photograph of micritic limestone infilling a fracture and interpillow space (interval 187-1155B-8R-3, 68–72 cm).

Figure 7. Poorly sorted and matrix supported basaltic breccia. Only clasts of basaltic derivation are visible in the breccia; included are basalt, palagonite ± glass ± spherulites, olivine (rare), and plagioclase (interval 187-1161A-5R-1, 83–113 cm).

Figure 8. Close-up photograph of interval 187-1156A-2R-2 (Piece 4, 14–20 cm). Basalt clasts with variably palagonitized glasses in a matrix of calcareous sediment.

Figure 9. Microcrystalline aphyric basalt typical of Hole 1161B (interval 187-1161B-3R-1, 54–59 cm).

Figure 10. Close-up photograph of interval 187-1154A-3R-1, 120–130 cm. Light gray, moderately plagioclase-olivine phyric pillow basalt, typical of that recovered throughout Hole 1154. Black irregular patches were formed by the plucking of altered groundmass from the cut surface.

Figure 11. Plagioclase + olivine glomerocryst showing intergrown prismatic plagioclase and skeletal olivine phenocrysts (Sample 187-1157B-6R-1, 43–47 cm).

Figure 12. Large euhedral plagioclase phenocrysts in a sparsely plagioclase-olivine phyric basalt (interval 187-1152B-5R-1, 107–114 cm).

Figure 13. Sieve-textured plagioclase, indicative of partial resorption and disequilibrium between it and the host basalt (Sample 187-1164B-2R-1, 50–53 cm; cross-polarized light).

Figure 14. Photomicrograph of clinopyroxene plumose quench texture in Sample 187-1152B-2R-1, 8–10 cm. Note the replacement of groundmass mesostasis by smectite.

Figure 15. Subophitic texture: the clinopyroxene shown is one crystal but has strain extinction and subtly separate domains (Sample 187-1158C-2R-1 [Piece 13, 75–78 cm]; cross-polarized light).

Figure 16. Interval 187-1161A-3R-1, 67–80 cm, showing fractures lined with cryptocrystalline silica within chilled margin of a pillow fragment. The inner spherulitic zone is highlighted as a result of partial replacement by clay.

Figure 17. Fe oxyhydroxide highlighting spherulitic zone in a pillow margin. Note the sediment fracture infill (interval 187-1153A-8R-1, 110–122 cm).

Figure 18. Concentric alteration halos progressing from a more intensely altered margin to a less intensely altered interior of a sparsely phyric basalt piece. The chilled margin and alteration halo are thicker in the top of the piece (interval 187-1152-6R-1, 33–40.5 cm).

Figure 19. Photomicrograph showing the transition from smectite/Fe oxyhydroxide groundmass replacement to a virtually unaltered groundmass at the alteration halo boundary (Sample 187-1156A-3R-2, 73–77 cm).

Figure 20. Glassy pillow rind consisting of fresh glass, palagonite, and silica veins (Sample 187-1153A-8R-1, 102–106 cm).

Figure 21. Photomicrograph of the intersection of calcite veins with palagonite. Silica, Fe oxyhydroxides, and Mn oxide line the edges of the calcite vein. Palagonite is altered to clay along dendritic alteration front. The vertical fracture within the palagonite contains Mn/Fe oxyhydroxides and silica (Sample 187-1155B-2R-1, 68–71 cm).

Figure 22. Close-up photograph of interval 187-1157B-3R-1, 137–147 cm. Calcite veins sporadically lined with thin silica selvages are surrounded by symmetric alteration halos in which the groundmass and olivine phenocrysts are largely replaced by smectite and Fe oxyhydroxide. Spotty Mn oxide is common within the calcite veins and along silica selvages.

Figure 23. **A**. Variations in $^{206}Pb/^{204}Pb$ along the Southeast Indian Ridge between 115°E and 140°E. The present position of the isotope boundary between Indian- and Pacific-type mid-ocean-ridge basalt (MORB) provinces is located at ~126°E. These data are taken from Klein et al. (1988), Pyle et al. (1992), and Pyle et al. (1995). ADD = Australian Antarctic Discordance. **B**. Variations of Zr/Ba vs. $^{206}Pb/^{204}Pb$ showing the data distribution that is used to determine Indian- and Pacific-type mantle provinces. These data are taken from Klein et al. (1988), Pyle et al. (1992, 1995), Pyle (1994), and D. Pyle and D. Christie (unpubl. data).

Figure 24. Distribution of MgO values in Hole 1160B. The hole passes through a sequence of seven flows in which pillow flows and massive flows alternate. Each massive flow is of the same lithology as the overlying pillow flow. Note the very similar high MgO contents of both glasses and massive flows. Whole-rock samples from the pillow flows have lost MgO during alteration.

Figure 25. **A**. Variations in Zr/Ba vs. Ba (in parts per million) content of basaltic glass dredged from 0- to 7-Ma seafloor within and east of the Australian Antarctic Discordance (ADD) (D. Pyle and D. Christie, unpubl. data). MORB = mid-ocean-ridge basalt; PRT = propagating rift tip lavas. **B**. Variations in Na_2O/TiO_2 vs. MgO (in weight percent) content of basaltic glass dredged from 0- to 7-Ma seafloor within and east of the AAD (D. Pyle and D. Christie, unpubl. data).

Figure 26. Average analyses for all Leg 187 glasses in relation to the 0- to 7-Ma data fields from Figure 25. **A**. Zr/Ba vs. Ba. Data are color coded according to the field in which they plot. Yellow triangles lie outside the 0- to 7-Ma fields and are referred to as Transitional Pacific because they appear to extend the Pacific field in the direction of Zone A propagating rift tip lava (PRT) compositions. The red triangle is a glass from Hole 1164A that plots at the boundary between the Pacific and Indian fields. MORB = mid-ocean-ridge basalt. **B**. Na_2O/TiO_2 vs. MgO. Color coding is defined by the Ba-Zr systematics in **A**. Note that no Leg 187 sample plots in the 0- to 7-Ma Indian field, but, with the exception of four Pacific samples, there is a clear division between Pacific and Indian samples. These four samples plot to the left of the B5 tie line in **A**, a region where small analytical errors in Ba result in large shifts in plotting position. Note also that Transitional-Pacific samples plot in both fields.

Figure 27. Site locations for Leg 187 in relation to seafloor isochrons (after Vogt et al., 1984). Sites are color coded according to the mantle domain from which their lavas were derived. Mantle domain interpretations are based on Figure 26A. Sites with two colors indicate that two types of mantle domains were sampled. Colored lines are ship tracks for Leg 187 and the two site survey cruises aboard the *R/V Melville*.

Figure 28. Leg 187 site locations in relation to the residual depth anomaly (gray contours) and SeaBeam bathymetry from the *Melville*'s Boomerang 5 site survey cruise. Sites colors are as in Figure 27. Base map after Christie et al. (1998).

Table 1. Summary of igneous petrology, Leg 187 (See table note. Continued on next page.)

Site	Age (Ma)	Hole	Mantle domain	Length (m)		Recovery (wt%)	Igneous lithology				Type of deposit	Unit description	Alteration
				Cored	Recovered		Aphyric	Sparsely pl-ol phyric	Moderately pl-ol phyric	Breccia			
1152	~25	A	Transitional Pacific	11.20	0.60	5.00	X				Talus	Unit 1: Aphyric basalt	Slight
		B	Transitional Pacific	23.70	3.60	15.15		(x)	X (cpx)		Talus Talus	Unit 1: Aphyric basalt Unit 2: Sparsely to moderately pl-ol-cpx phyric basalt	Slight
				Total:	4.20	12.03							
1153	~28	A	Pacific	7.30	1.77	24.25	X				Pillows	Unit 1: Aphyric basalt	Slight
				Total:	1.77	24.25							
1154	~28	A	Pacific	34.40	9.42	28.90			X		Pillows	Unit 1: Moderately pl-ol phyric basalt	Slight
				Total:	9.42	28.90							
1155	~24.5	A	Transitional Pacific	26.20	2.34	8.93	X		X		Pillows Talus	Unit 1: Moderately pl-ol phyric basalt Unit 2: Aphyric basalt with moderately pl-ol phyric basalt (i.e., basaltic rubble)	Slight to moderate
		B	Transitional Pacific	46.00	18.18	39.52			X	CCV	Pillows into sediments	Unit 1: Moderately pl-ol phyric basalt (micritic sediments + lithics in fractures)	High at top Slight at bottom
				Total:	20.52	28.42							
1156	~22	A	Indian	11.40	6.30	55.26		(x)	X	X (Cc) CCV	Talus Pillows	Unit 1: Breccia of phyric basalt Unit 2: Sparsely to moderately pl-ol phyric basalt with carbonate sediments	Slight
		B	Indian	33.60	9.92	29.52			X		Unknown	Unit 1: Moderately to highly pl-ol phyric basalt	Slight to moderate
				Total:	16.22	36.04							
1157	~22.5	A	Indian	16.40	2.92	17.80	X		X	X (Cc) CCV	Rubble	Unit 1: Basaltic rubble (aphyric and pl-ol phyric basalt with carbonate sediments)	Slight to moderate
		B	Indian	40.40	11.70	28.96			X		Pillows	Unit 1: Moderately pl-ol phyric basalt	Slight to moderate
				Total:	14.62	25.74							
1158	~21	A	Pacific	14.40	0.85	5.90	X	X			Rubble (pillows)	Unit 1: Aphyric to sparsely ol-pl phyric basalt	Slight to moderate
		B	Pacific	15.00	1.60	10.67	X	X			Rubble? (flow/dike)	Unit 1: Aphyric to sparsely ol-pl phyric basalt (fine grained)	Slight to moderate
		C	Pacific	9.90	1.61	17.13	X	X			Flow/dike?	Unit 1: Aphyric to sparsely ol-pl phyric basalt Unit 2: Diabase (with aphyric basalt)	Slight to moderate
				Total:	4.06	10.33							
1159	~14	A	Pacific	27.70	7.96	28.74	X			X (Si)	Pillows	Unit 1: Aphyric basalt (+ hyaloclastites)	Slight to moderate
				Total:	7.96	28.74							
1160	~21.5	A	Pacific	5.10	0.43	8.43	X		X		Rubble (pillows)	Unit 1: Aphyric basalt	Slight to moderate

Site	Age (Ma)	Hole	Mantle domain	Length (m)		Recovery (wt%)	Igneous lithology				Type of deposit	Unit description	Alteration
				Cored	Recovered		Aphyric	Sparsely pl-ol phyric	Moderately pl-ol phyric	Breccia			
		B	Pacific	45.10	13.01	28.85	X		X		Pillows Massive Pillows Massive Pillows Massive Pillows	Unit 1: Aphyric basalt (microcrystalline) Unit 2: Aphyric basalt (fine grained) Unit 3: Moderately pl-(ol) basalt (microcrystalline) Unit 4: Moderately pl-ol phyric basalt (fine grained) Unit 5: Moderately pl-ol basalt (microcrystalline) Unit 6: Moderately pl phyric basalt (fine grained) Unit 7: Aphyric basalt (microcrystalline)	Slight to moderate Slight Slight to moderate Slight Slight to moderate Slight Slight to moderate
				Total:	13.44	26.77							
1161	~19	A	Indian	29.30	4.39	14.98	X	X	X	X (Si)	Talus	Unit 1: Basaltic rubble (sparsely pl-ol phyric basalt, moderately pl-ol phyric basalt, fine-grained aphyric basalt with Si-clay-cemented breccia)	Moderate to high
		B	Indian	8.50	0.86	10.12	X	X	X	X (Si)	Talus	Unit 1: Basaltic rubble (microcrystalline aphyric basalt, sparsely pl-ol phyric basalt, moderately pl-ol phyric basalt, fine-grained aphyric basalt with Si-clay-cemented breccia)	Moderate to high
				Total:	5.25	13.89							
1162	~18	A	Pacific	31.40	2.58	8.22	(x)		(x)	X (Dc)	Fault Breccia?	Unit 1: Mixed igneous clasts (metabasalt) Unit 2: Dolomite-cemented breccia (basalt, metadiabase, cataclasite)	High
		B	Pacific	58.90	9.94	16.88	(x)		(x)	X (Dc)	Fault Breccia?	Unit 1: Dolomite limestone (with lithics) Unit 2: Dolomite-cemented breccia (aphyric and phyric basalt)	High
				Total:	12.52	13.86							
1163	~16	A	Transitional Pacific	47.10	15.70	33.33	X		X	X (Cc) CCV	Pillows	Unit 1: Moderately pl-ol phyric basalt Unit 2: Aphyric basalt with carbonate sediments	Slight to moderate Slight to moderate
				Total:	15.70	33.33							
1164	~17	A	Transitional Pacific	8.50	0.97	11.41	X (cpx)				Rubble?	Unit 1: Aphyric basalt (pl-cpx microphenocryst)	Slight to moderate
		B	Transitional Pacific	65.70	10.65	16.21	X	X	X	X (Si)	Rubble (pillows)	Unit 1: Basaltic rubble (aphyric and pl-ol phyric basalt with Si-clay-cemented breccia)	Slight to high
				Total:	11.62	15.66							
	Cruise totals:			617.20	137.30	22.25							

Note: pl = plagioclase, ol = olivine, cpx = clinopyroxene, CCV = composite carbonate vein, X = major lithology, (x) = minor lithology, Cc = calcite cemented, Dc - dolomite cemented, and Si = silica.

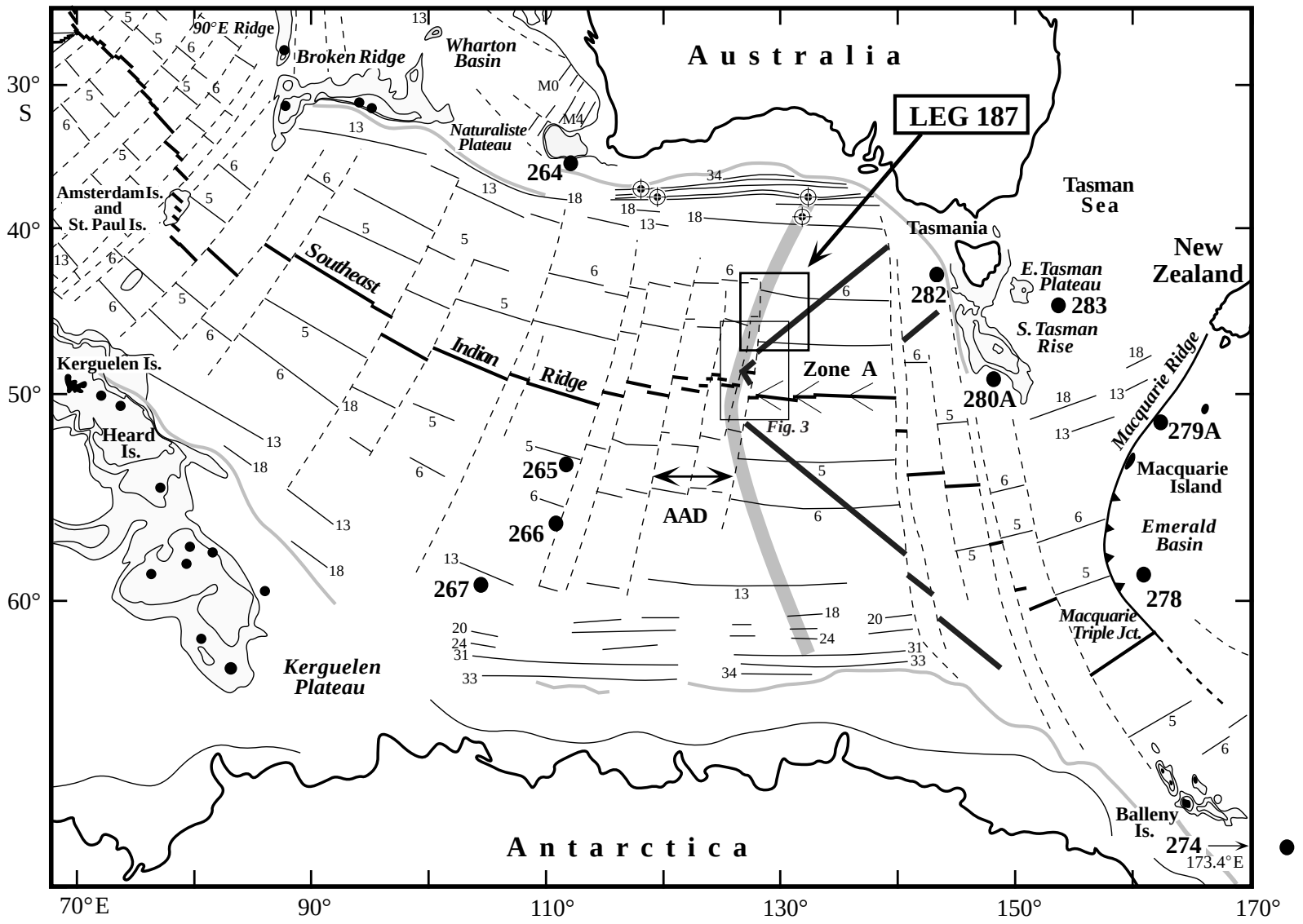
90°E Ridge
Broken Ridge
Wharton Basin
Australia
LEG 187
Naturaliste Plateau
264
Tasman Sea
Amsterdam Is. and St. Paul Is.
Southeast Indian Ridge
Tasmania
New Zealand
E. Tasman Plateau
282
283
S. Tasman Rise
Zone A
280A
Fig. 3
Macquarie Ridge
279A
Kerguelen Is.
Heard Is.
265
AAD
Macquarie Island
266
Emerald Basin
267
278
Macquarie Triple Jct.
Kerguelen Plateau
Balleny Is.
274
173.4°E
Antarctica
30° S
40°
50°
60°
70°E
90°
110°
130°
150°
170°

Figure 1

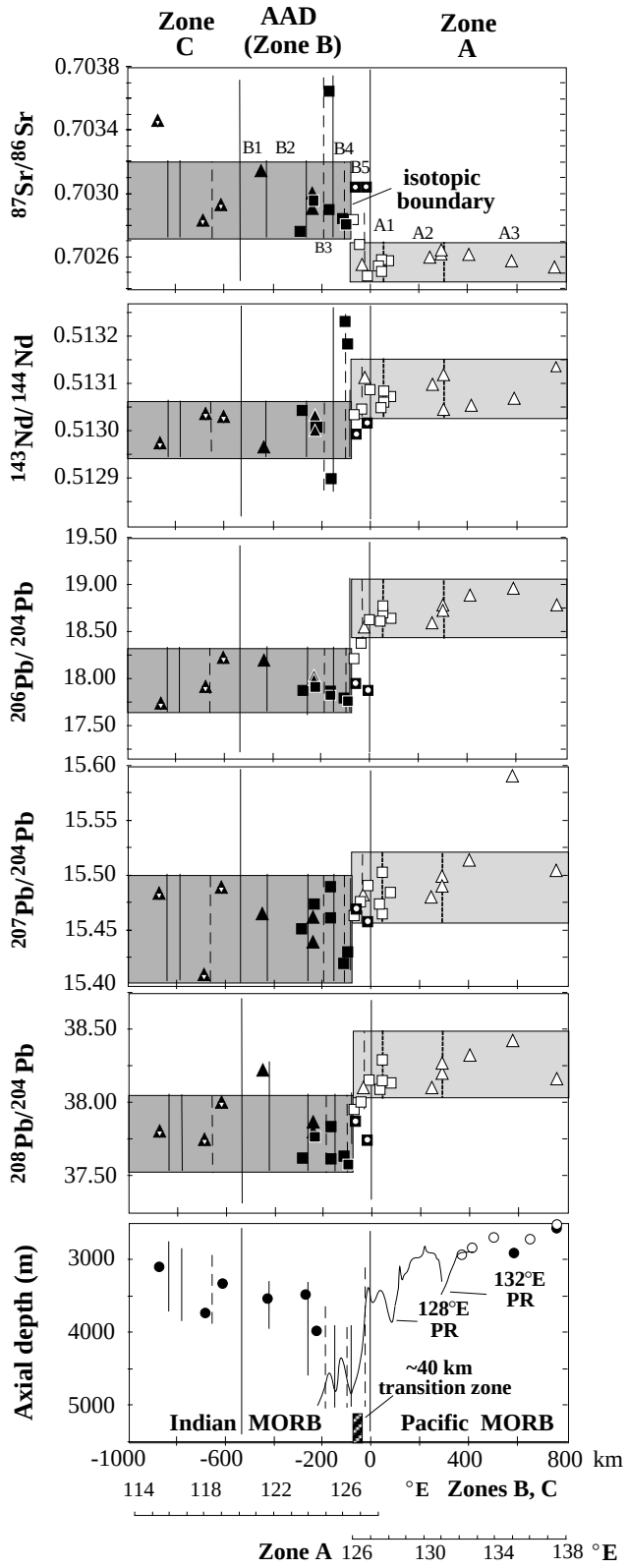
Zone C
AAD (Zone B)
Zone A
$^{87}Sr/^{86}Sr$
0.7038
0.7034
0.7030
0.7026
B1
B2
B4
B5
B3
A1
A2
A3
isotopic boundary
$^{143}Nd/^{144}Nd$
0.5132
0.5131
0.5130
0.5129
$^{206}Pb/^{204}Pb$
19.50
19.00
18.50
18.00
17.50
$^{207}Pb/^{204}Pb$
15.60
15.55
15.50
15.45
15.40
$^{208}Pb/^{204}Pb$
38.50
38.00
37.50
Axial depth (m)
3000
4000
5000
132°E PR
128°E PR
~40 km transition zone
Indian MORB
Pacific MORB
-1000
-600
-200
0
400
800 km
114
118
122
126
°E Zones B, C
Zone A
126
130
134
138 °E

Figure 2

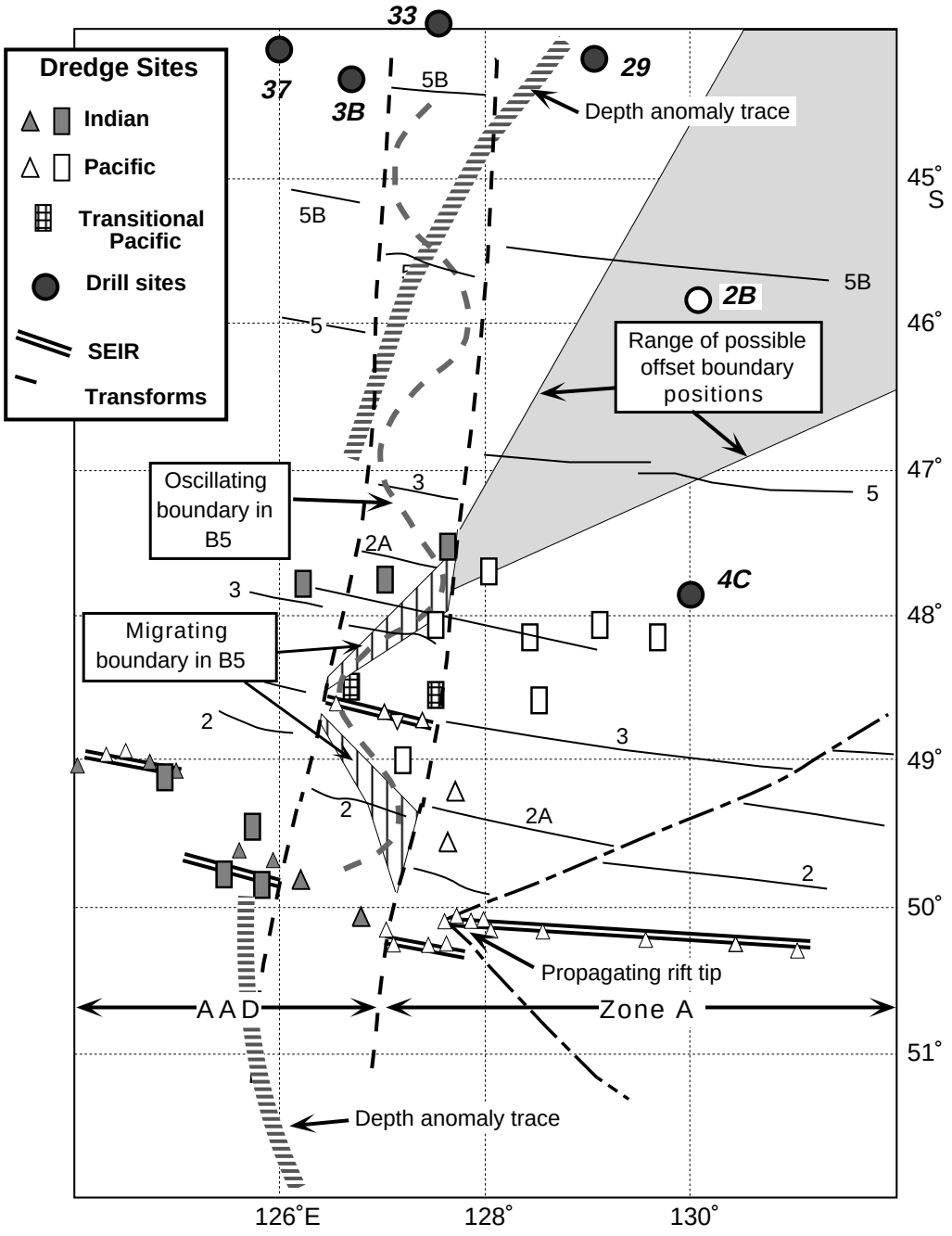
Dredge Sites
Indian
Pacific
Transitional Pacific
Drill sites
SEIR
Transforms
33
37
3B
29
2B
4C
Depth anomaly trace
Range of possible offset boundary positions
Oscillating boundary in B5
Migrating boundary in B5
Propagating rift tip
Depth anomaly trace
AAD
Zone A
5B
5
3
2A
2
45° S
46°
47°
48°
49°
50°
51°
126°E
128°
130°

Figure 3

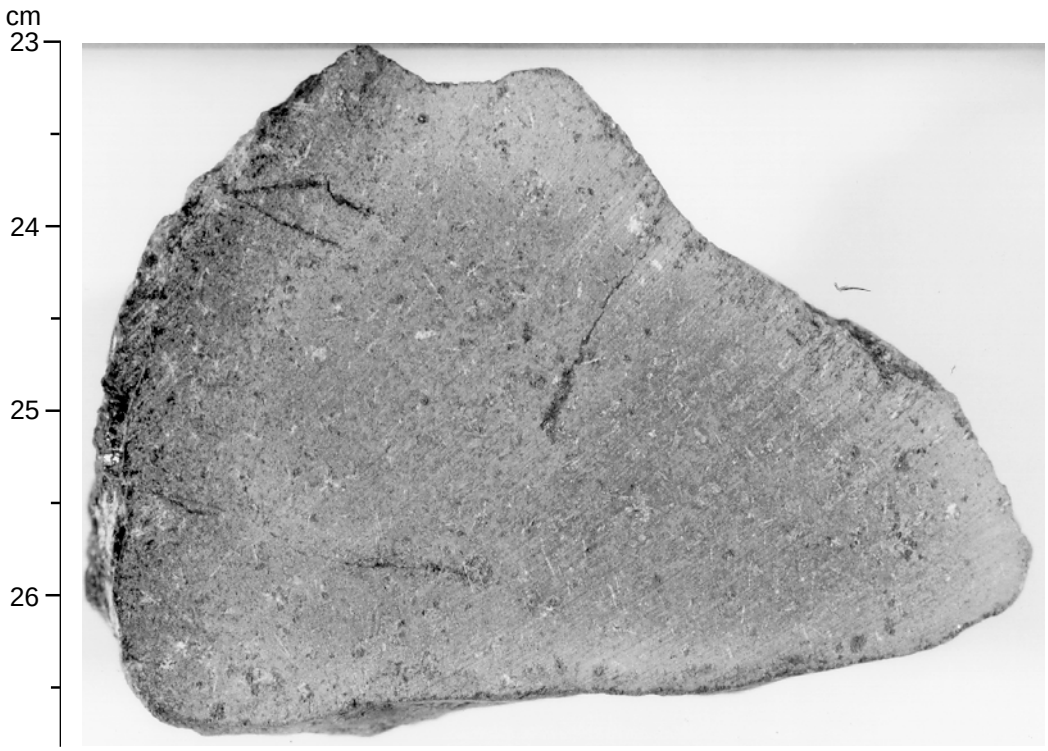

Figure 4

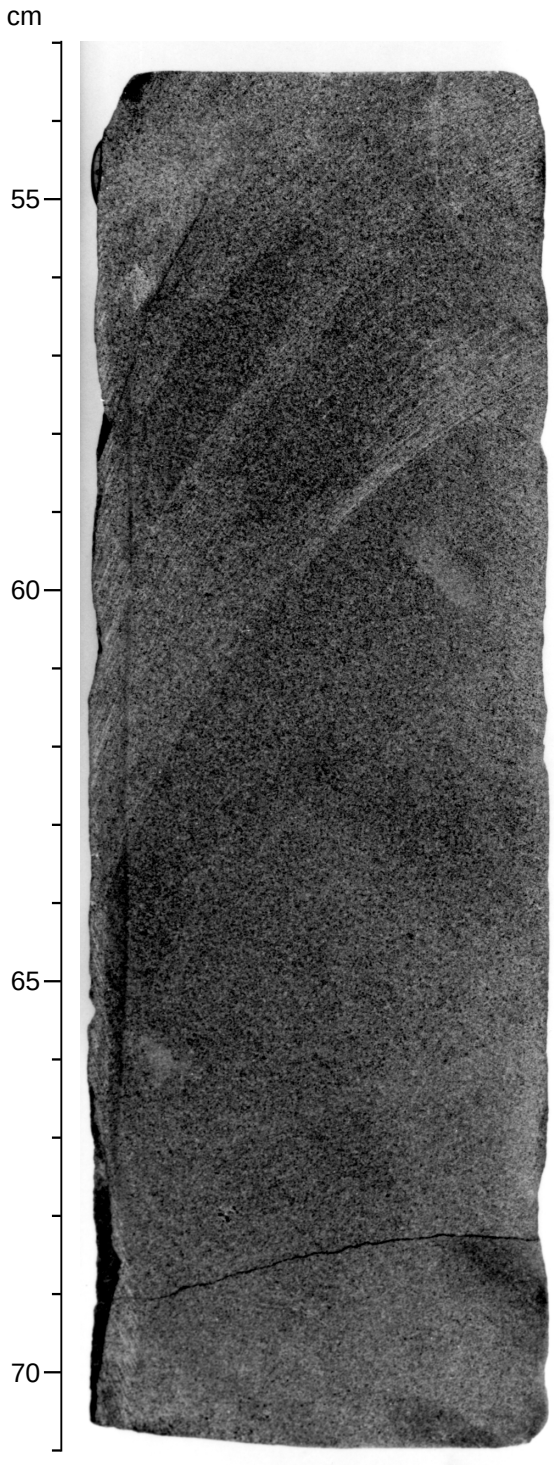

Figure 5

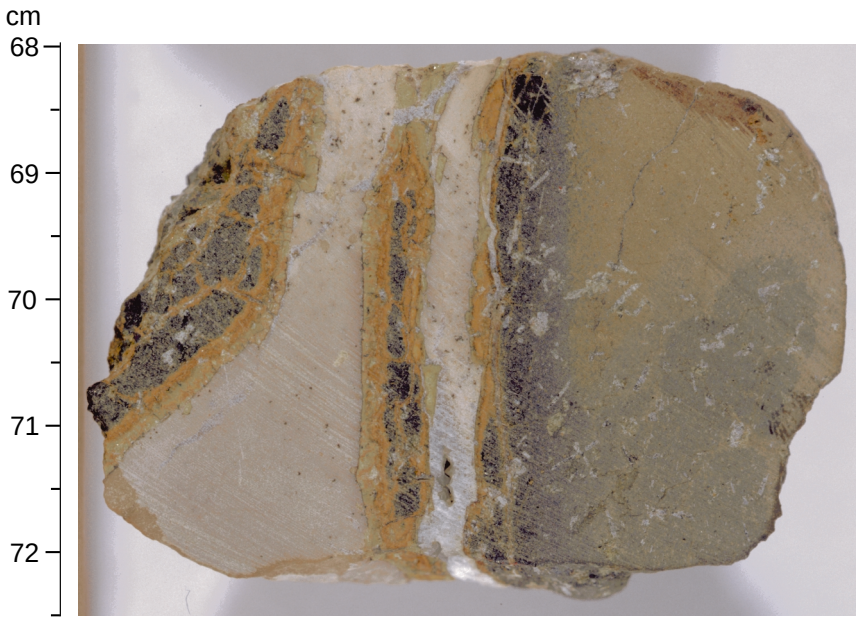

Figure 6

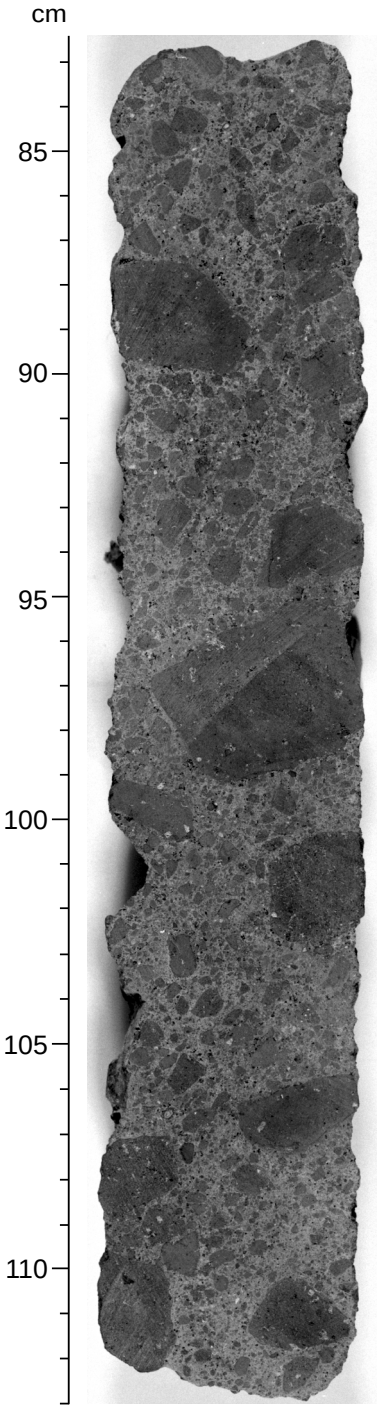

Figure 7

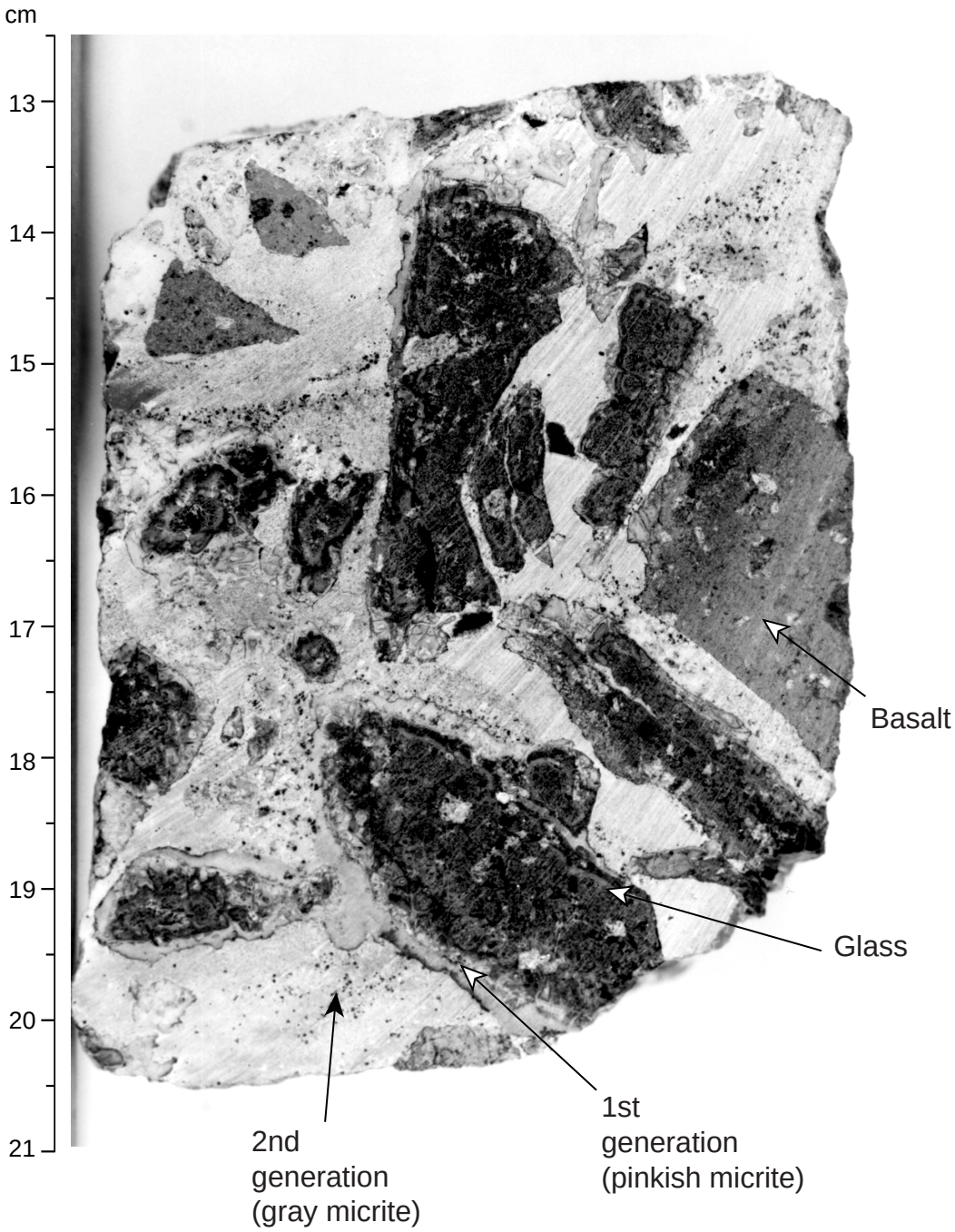
cm
13
14
15
16
17
18
19
20
21
Basalt
Glass
1st
generation
(pinkish micrite)
2nd
generation
(gray micrite)

Figure 8

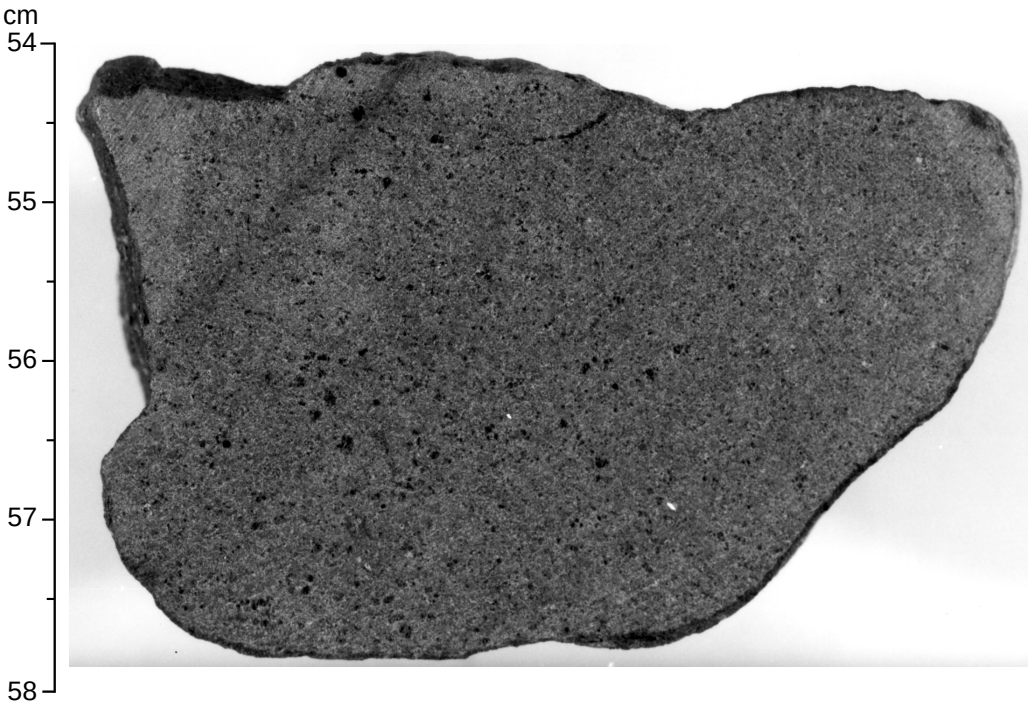

Figure 9

Figure 10

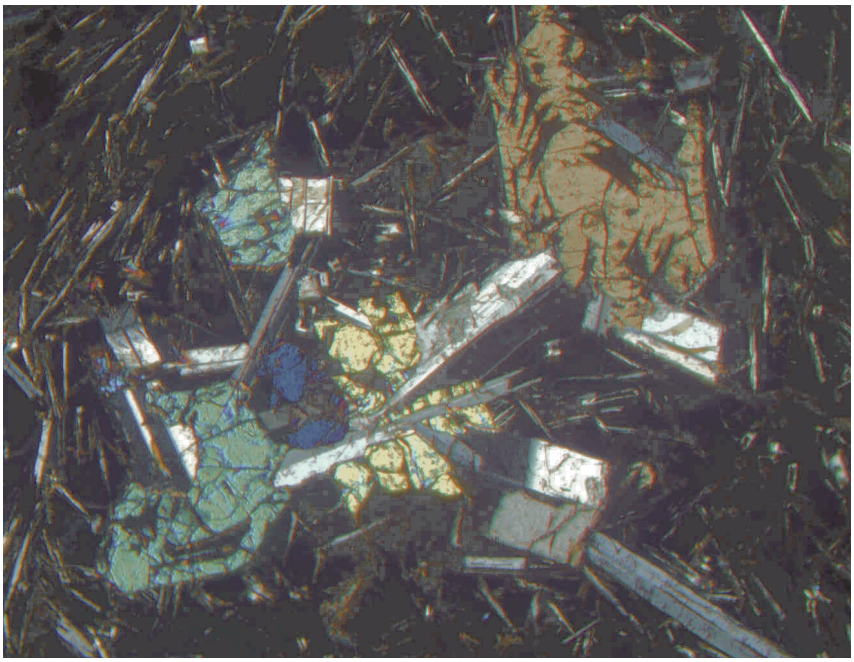

Figure 11

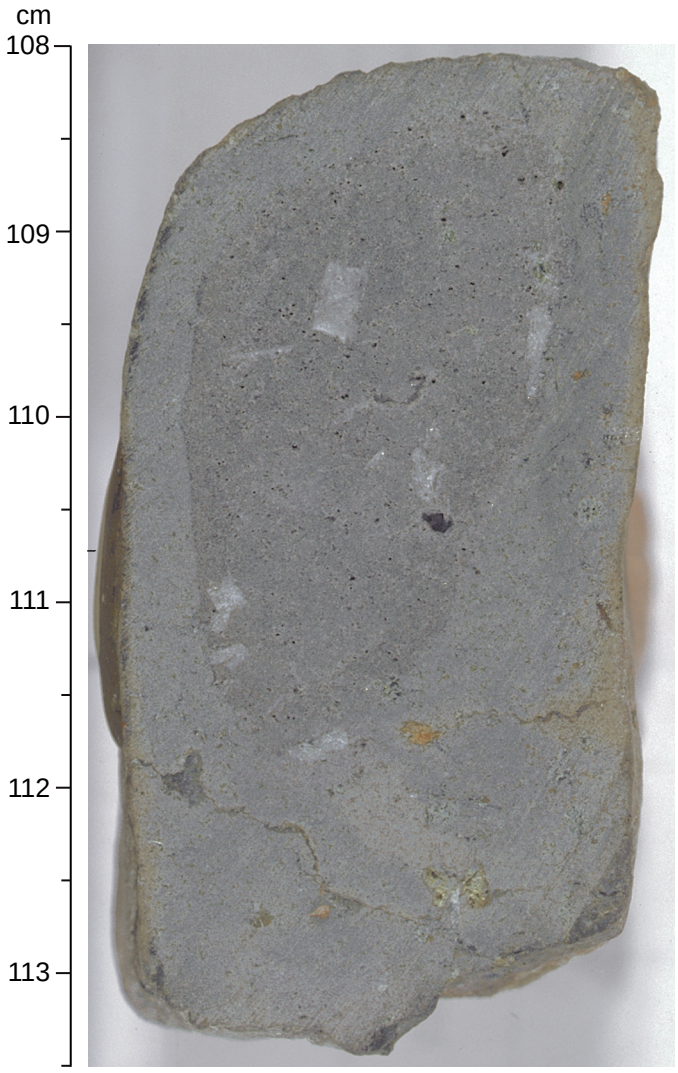

Figure 12

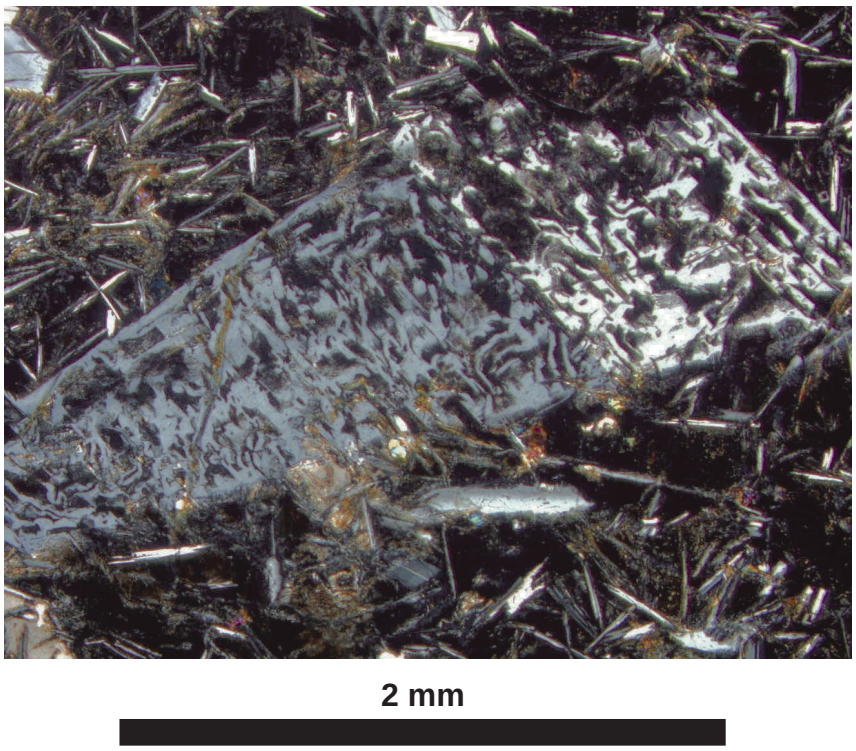

Figure 13

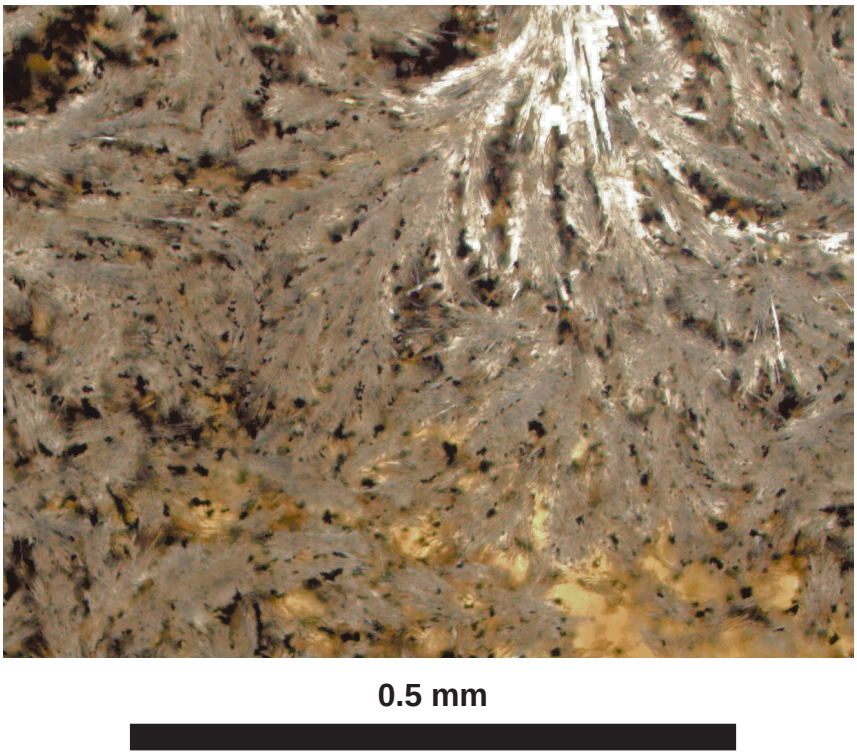

Figure 14

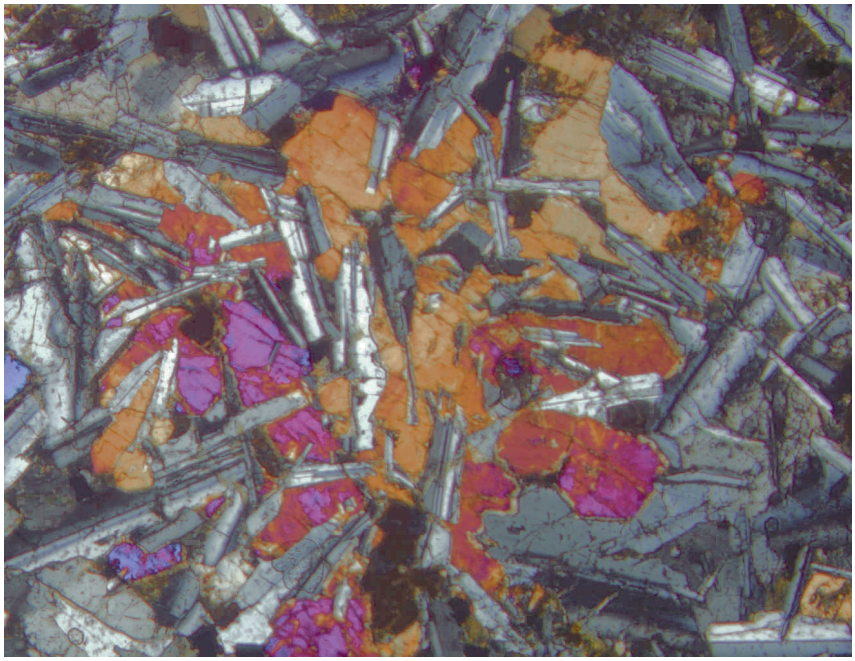

Figure 15

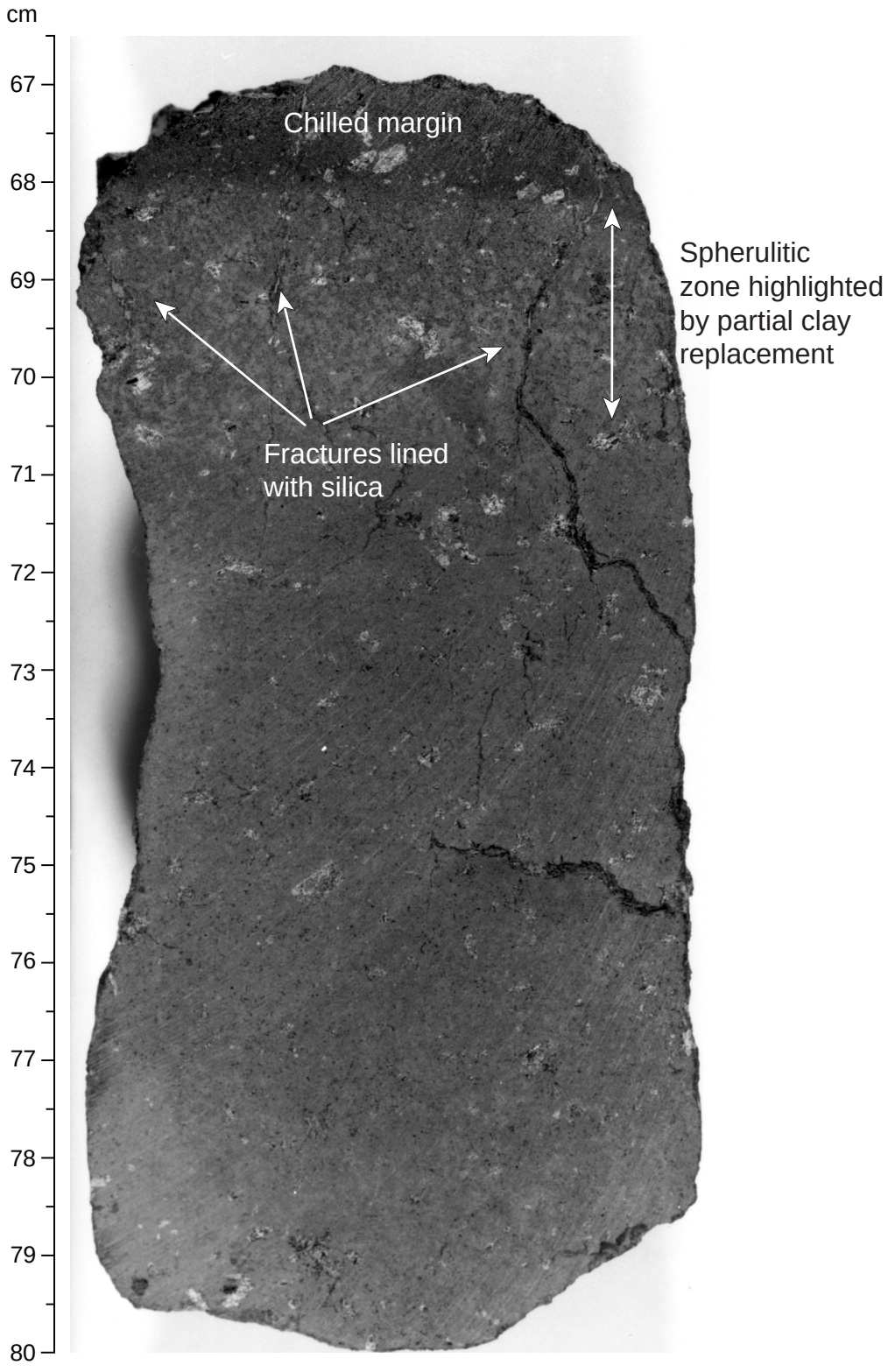
cm
67
68
69
70
71
72
73
74
75
76
77
78
79
80
Chilled margin
Spherulitic zone highlighted by partial clay replacement
Fractures lined with silica

Figure 16

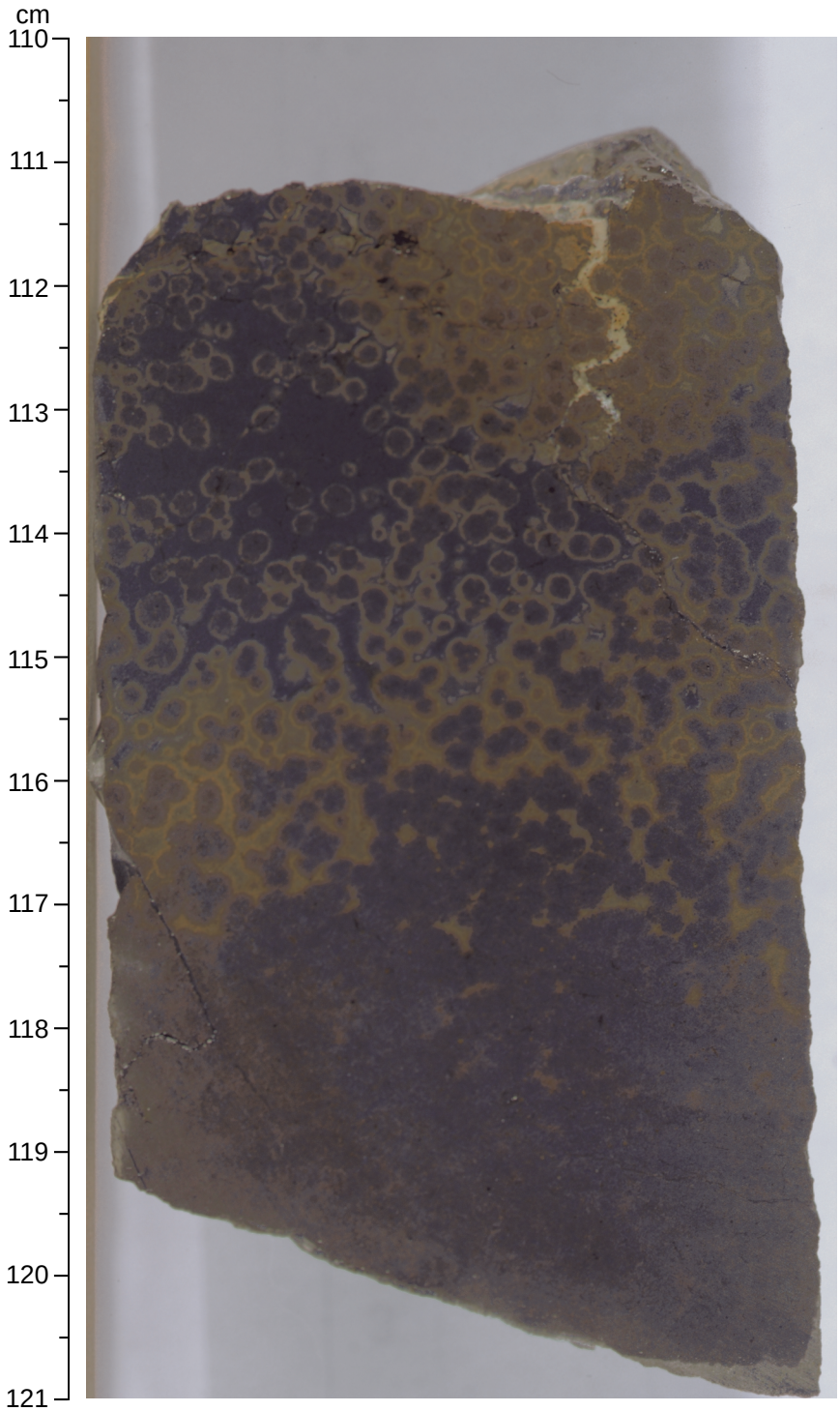

Figure 17

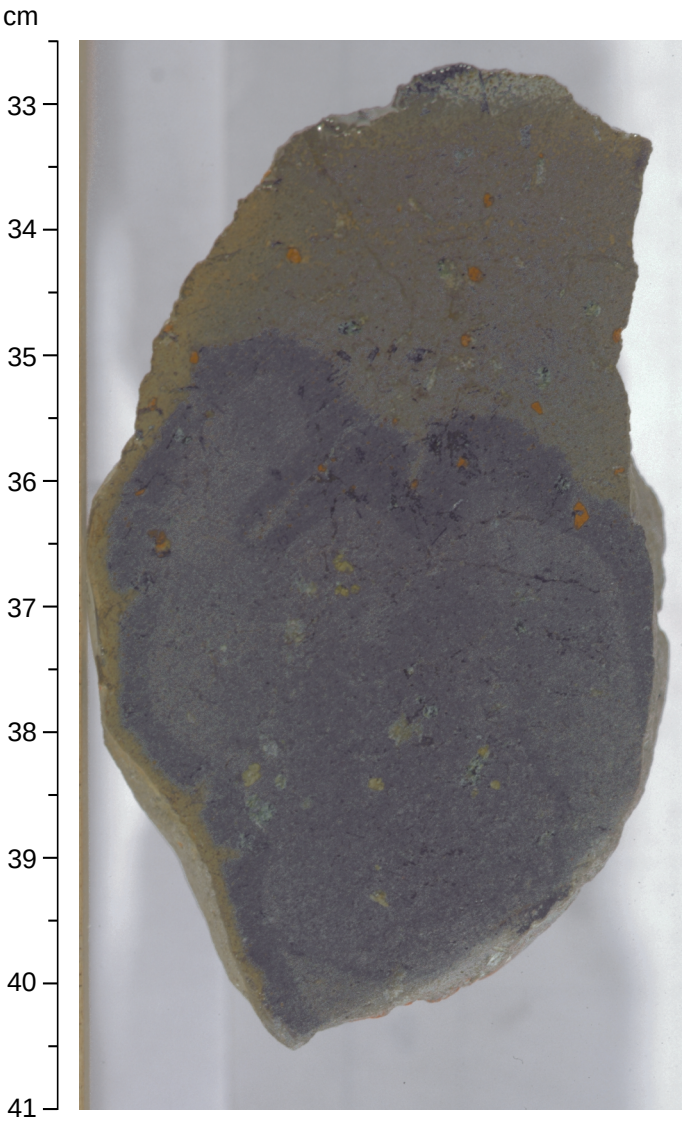

Figure 18

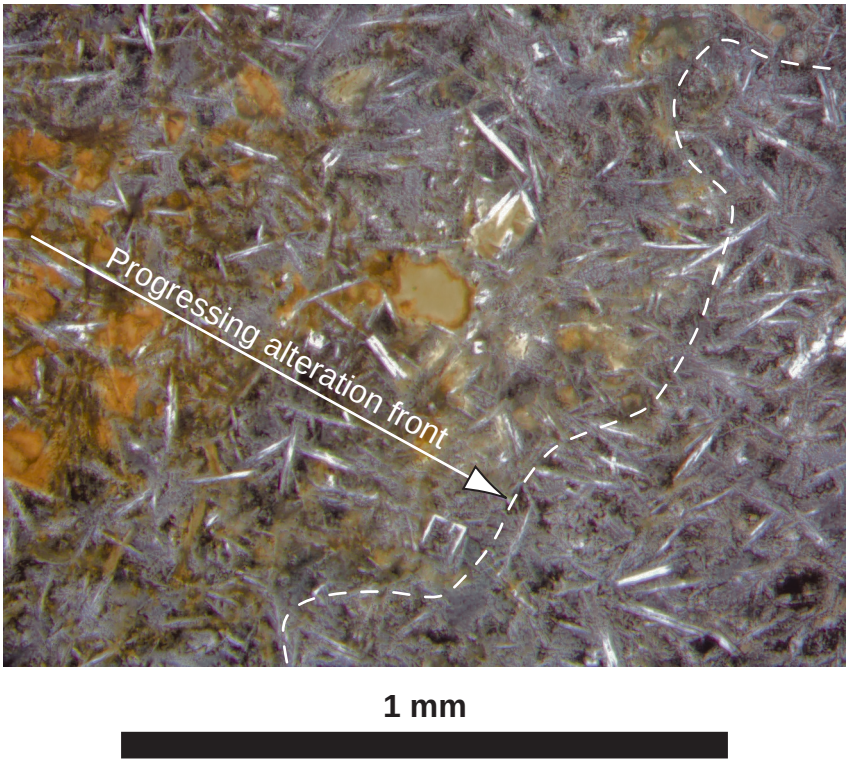

Figure 19

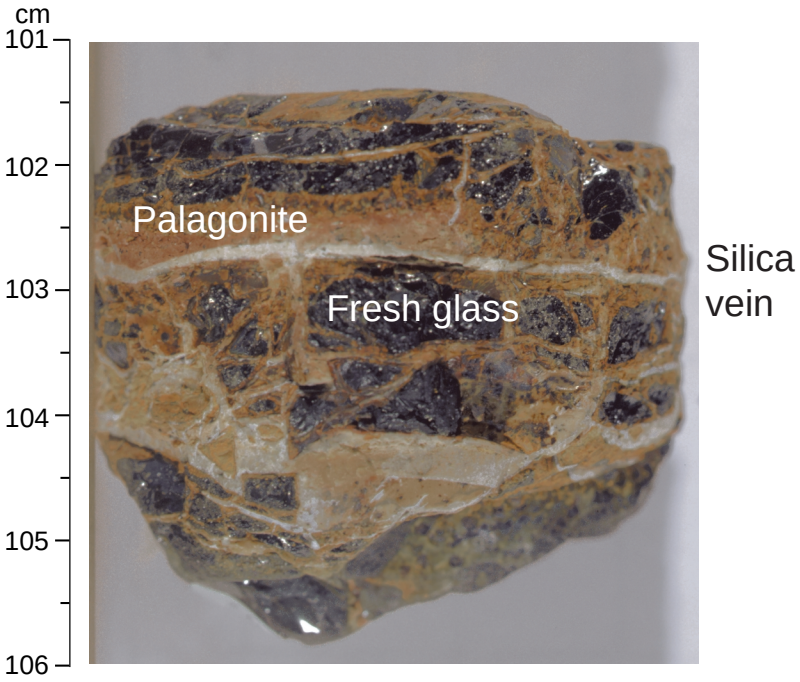
cm
101
102
103
104
105
106
Palagonite
Fresh glass
Silica
vein

Figure 20

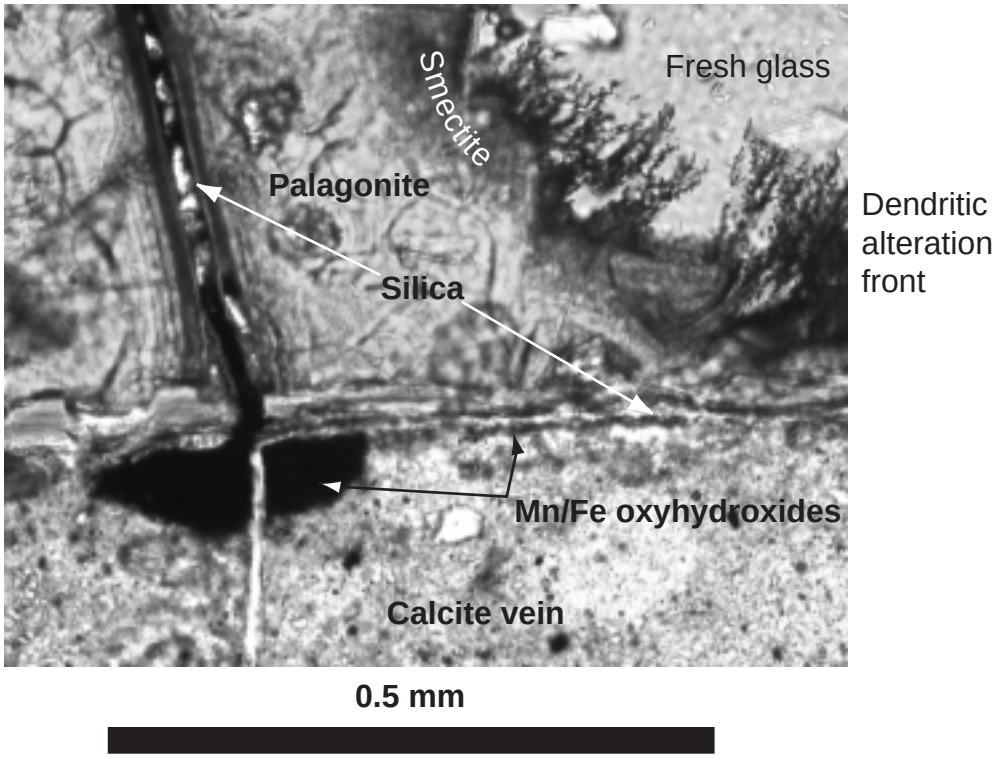
Fresh glass
Smectite
Palagonite
Silica
Dendritic
alteration
front
Mn/Fe oxyhydroxides
Calcite vein
0.5 mm

Figure 21

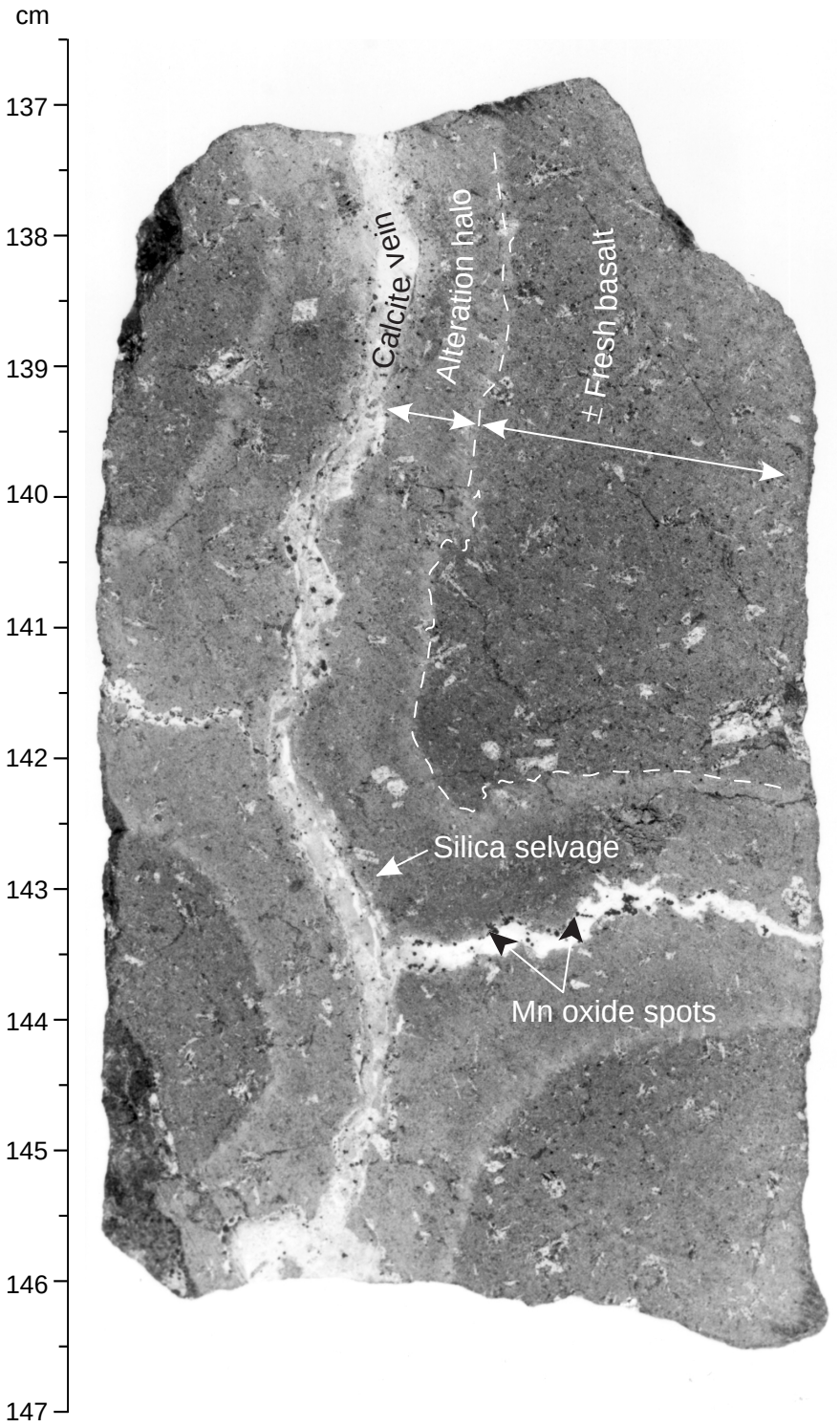
cm
137
138
139
140
141
142
143
144
145
146
147
Calcite vein
Alteration halo
± Fresh basalt
Silica selvage
Mn oxide spots

Figure 22

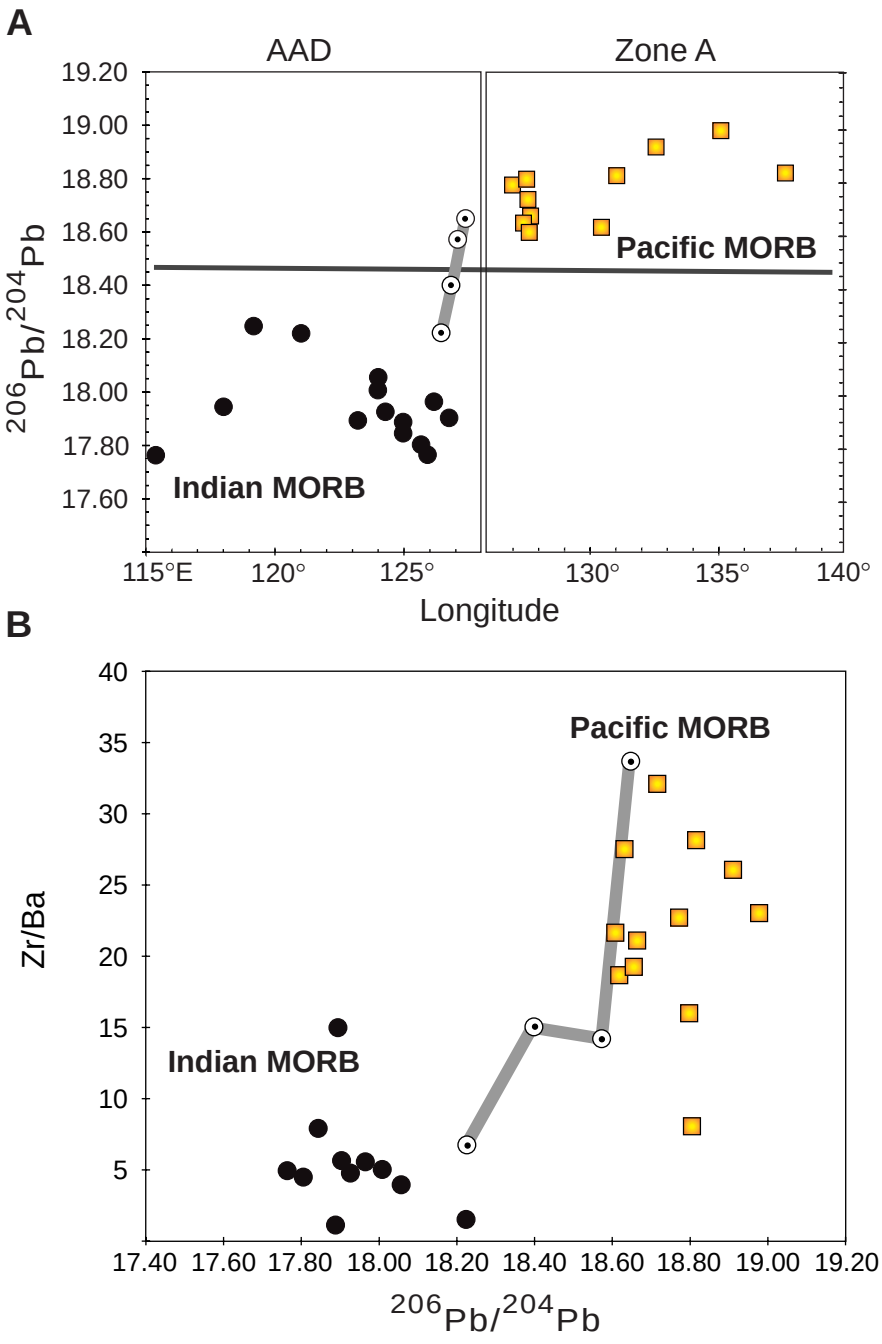
A
AAD
Zone A
Pacific MORB
Indian MORB
$^{206}Pb/^{204}Pb$
19.20
19.00
18.80
18.60
18.40
18.20
18.00
17.80
17.60
115°E
120°
125°
130°
135°
140°
Longitude
B
Pacific MORB
Indian MORB
Zr/Ba
40
35
30
25
20
15
10
5
17.40
17.60
17.80
18.00
18.20
18.40
18.60
18.80
19.00
19.20
$^{206}Pb/^{204}Pb$

Figure 23

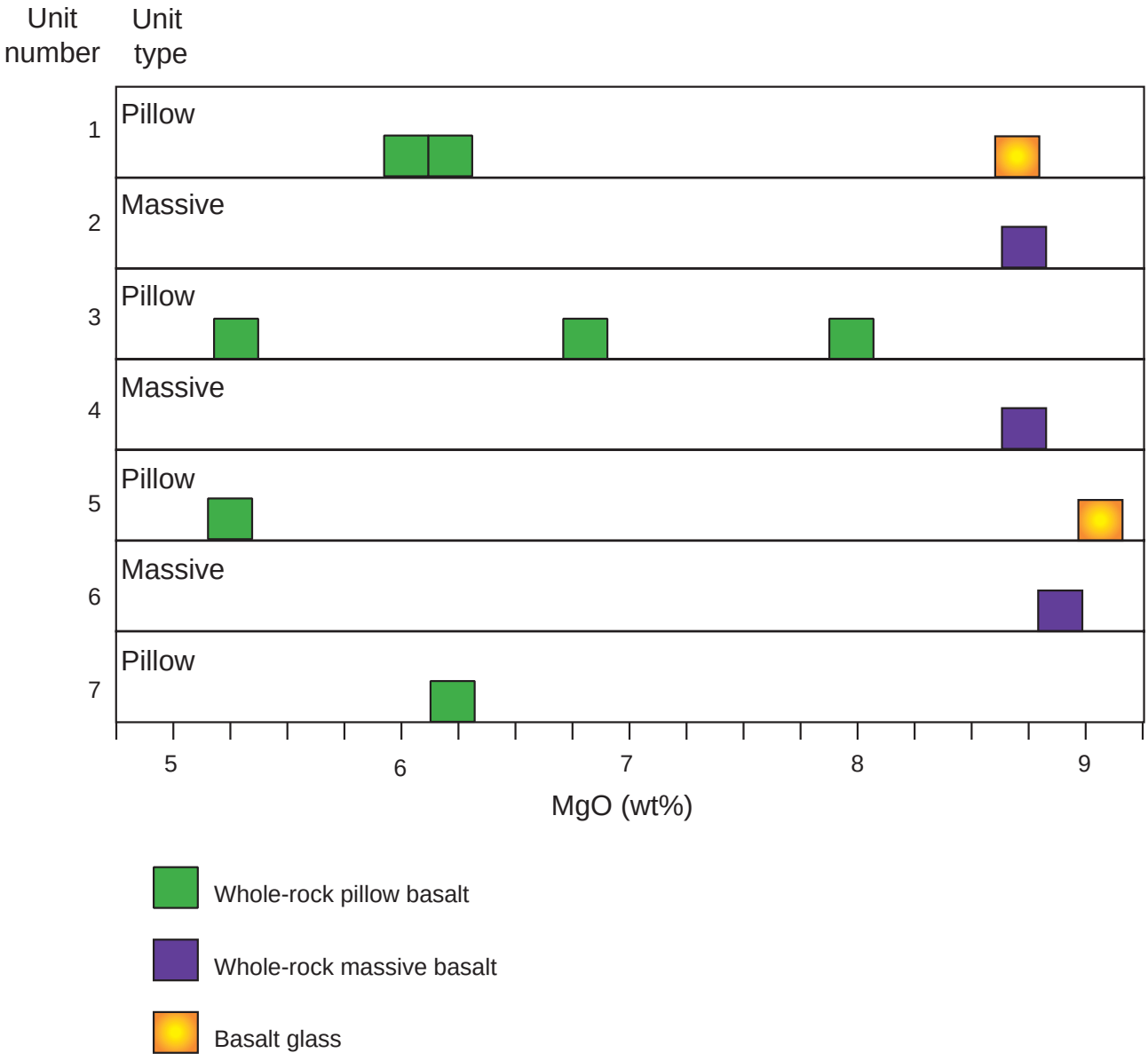
Unit number
Unit type
1
Pillow
2
Massive
3
Pillow
4
Massive
5
Pillow
6
Massive
7
Pillow
5
6
7
8
9
MgO (wt%)
Whole-rock pillow basalt
Whole-rock massive basalt
Basalt glass

Figure 24

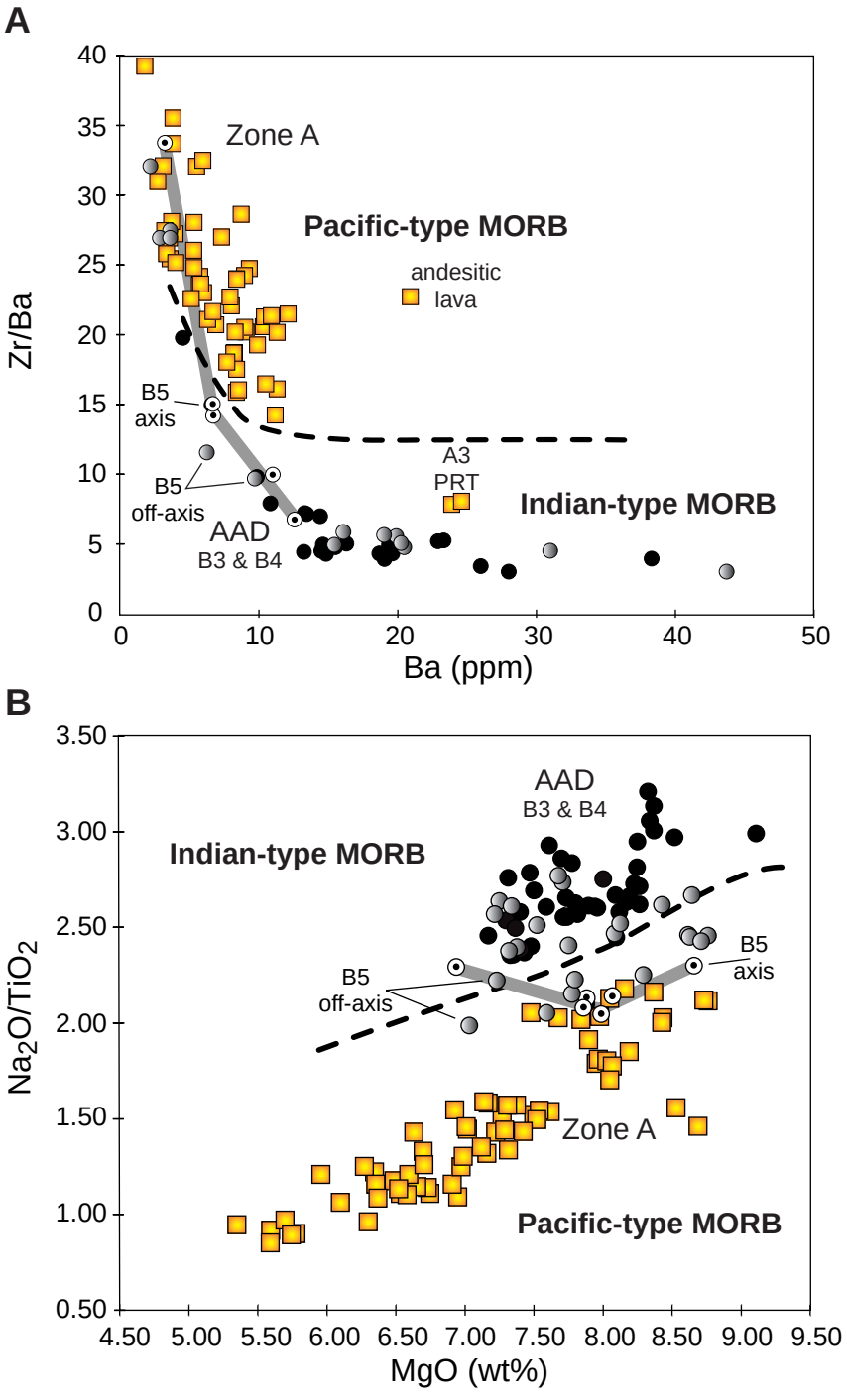
A
Zr/Ba
Ba (ppm)
Zone A
Pacific-type MORB
andesitic
lava
B5
axis
B5
off-axis
AAD
B3 & B4
A3
PRT
Indian-type MORB
B
Na2O/TiO2
MgO (wt%)
AAD
B3 & B4
Indian-type MORB
B5
axis
B5
off-axis
Zone A
Pacific-type MORB

Figure 25

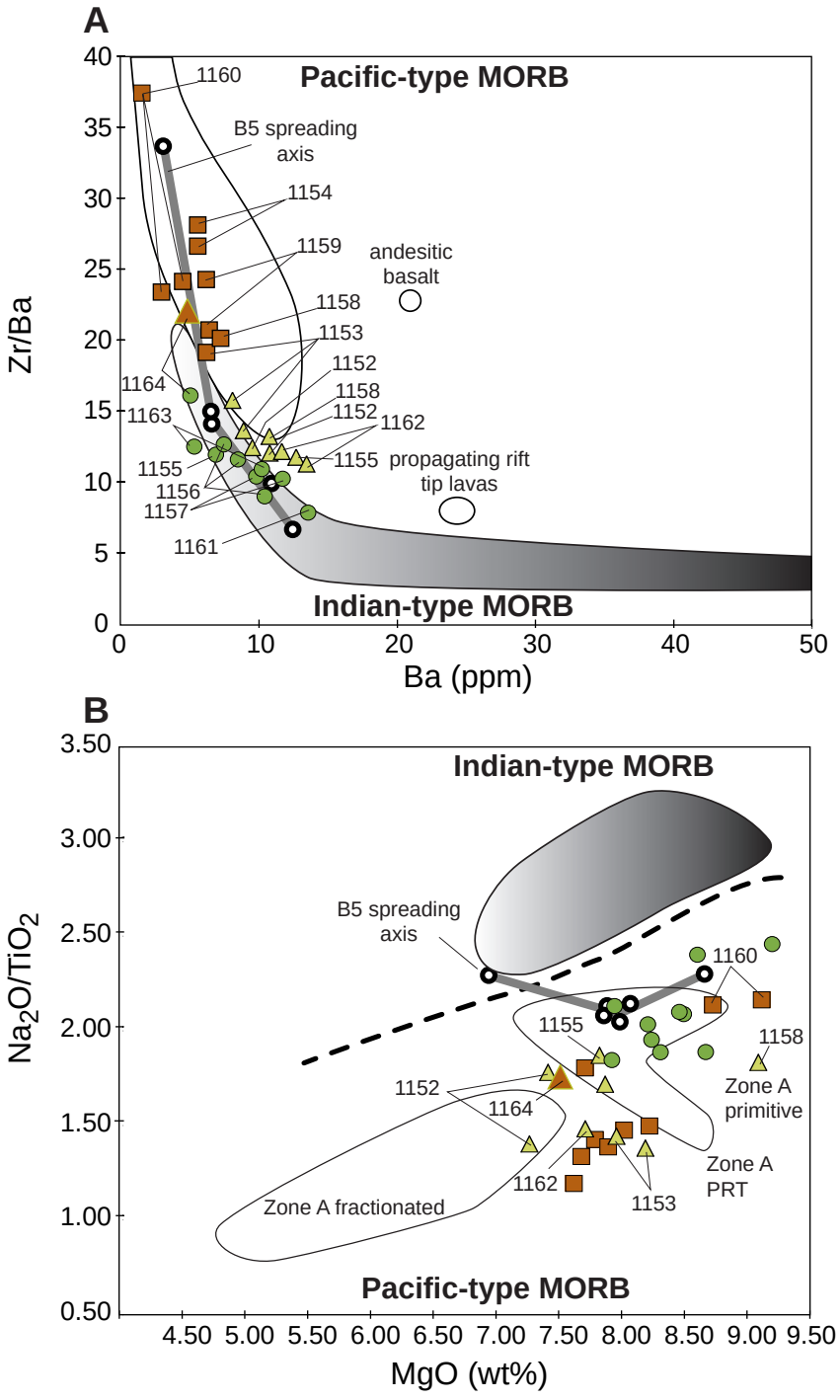
A
Pacific-type MORB
B5 spreading axis
andesitic basalt
propagating rift tip lavas
Indian-type MORB
Zr/Ba
Ba (ppm)
1160
1154
1159
1158
1153
1152
1164
1163
1155
1156
1157
1161
B
Indian-type MORB
B5 spreading axis
Zone A primitive
Zone A PRT
Zone A fractionated
Pacific-type MORB
Na2O/TiO2
MgO (wt%)

Figure 26

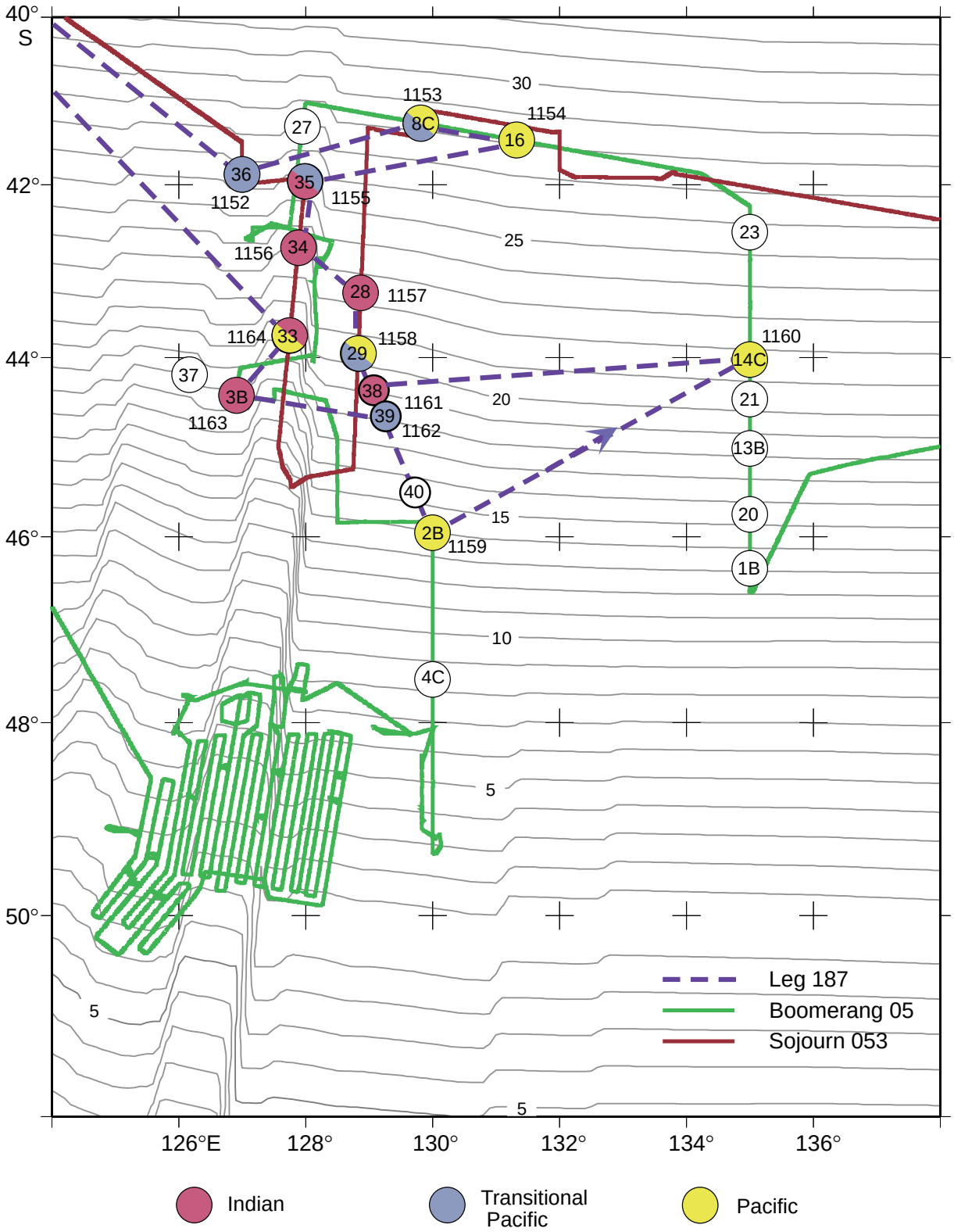
40° S
42°
44°
46°
48°
50°
126°E
128°
130°
132°
134°
136°
30
25
20
15
10
5
1153
1154
1152
1155
1156
1157
1164
1158
1160
1163
1161
1162
1159
27
8C
16
36
35
34
28
33
29
37
3B
38
39
40
2B
4C
23
14C
21
13B
20
1B
Leg 187
Boomerang 05
Sojourn 053
Indian
Transitional Pacific
Pacific

Figure 27

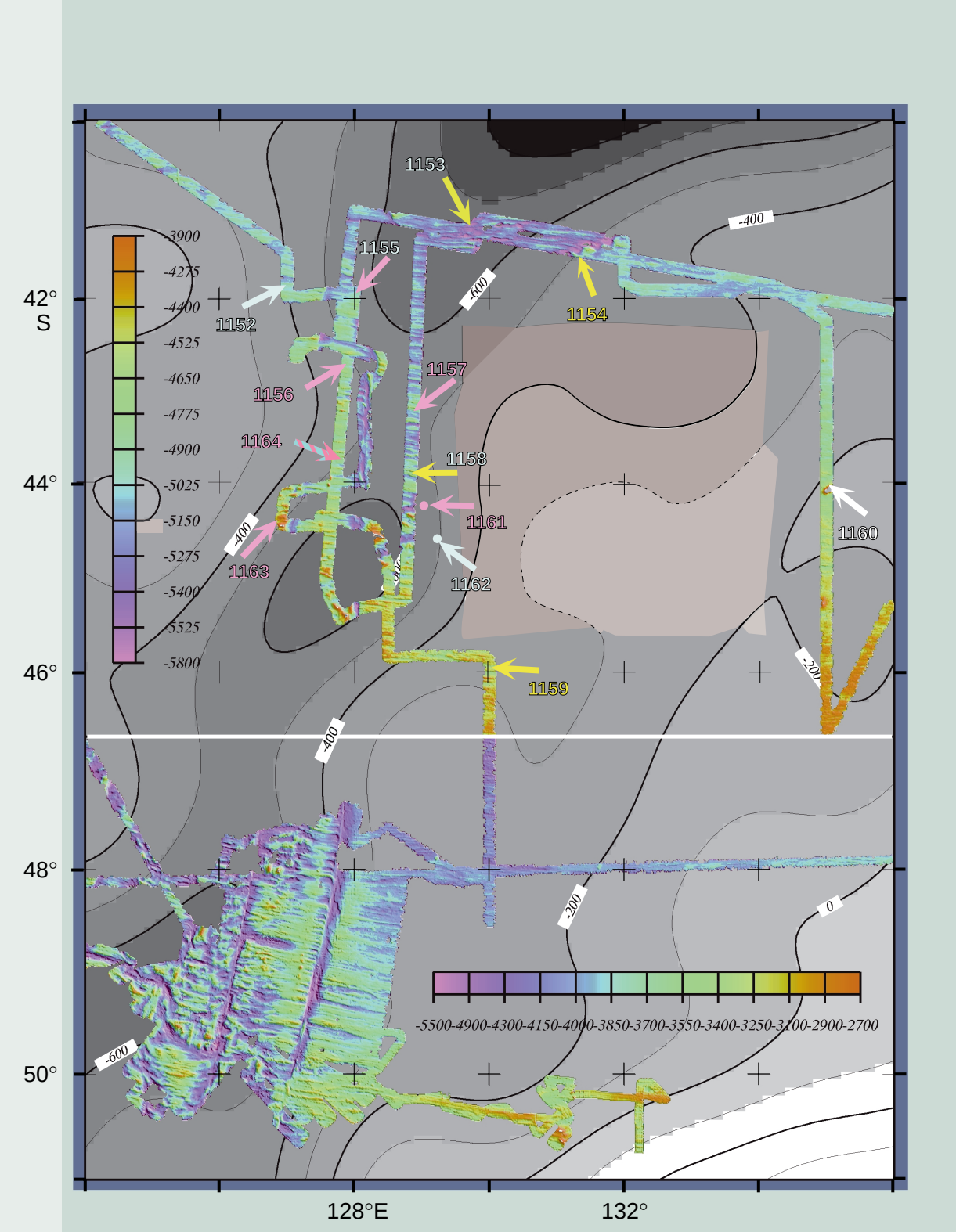

Base map produced by Bryan West, published in Christie et al., *Nature* (1998).

Figure 28

OPERATIONS SYNOPSIS[1]

PORT CALL

Fremantle

Leg 187 began at 1815 hr on 16 November 1999 when the first line was passed ashore to Berth "H" of Victoria Quay at Fremantle, Australia, at the conclusion of Leg 186ST. During the port call, several pieces of scientific apparatus were serviced (microscopes, X-ray fluorescence spectrophotometer, and cryogenic magnetometer), and the new inductively coupled plasma spectrophotometer was installed in the chemistry laboratory. The Ryan Energy Technology, Inc., Fusion rig instrumentation software installation, which was started in Singapore during the dry dock, was also completed. The drill crew finished the assembly and static testing of the passive and active components of the heave compensator by the morning of 21 November. The project was complicated by the discovery that a defective directional servo valve in the active compensator required replacement. A local Bosch supplier expedited a replacement part from Adelaide during the evening of 20 November. Our departure was also delayed because the Fremantle tugboat operators conducted a 48-hr work stoppage starting the morning of 19 November and lasting until 0900 hr on 21 November.

At 1210 hr on 21 November, the last line was released from the pier and the *JOIDES Resolution* was maneuvered into the channel. After the pilot departed the vessel at 1300 hr, the *JOIDES Resolution* began steaming at full speed on a southerly course.

TEST SITE

Transit to Test Site

Before proceeding to the first location of the leg, the ship was required to make a small diversion to a site off Albany in southwestern Australia. This was done in order to perform acceptance testing of the newly installed active heave compensator and the Fusion rig instrumentation system. The brief testing period also allotted additional time for crew familiarization with the new systems. The 401-nmi journey was completed at an average speed of 9.6 kt in calm seas and under fair skies.

---

[1]The Operations and Engineering personnel aboard the *JOIDES Resolution* during Leg 187 were ODP Operations Manager Ron Grout, ODP Downhole Tools Specialist Mike Friedrichs, and Schlumberger Engineer Kerry Swain.

Test Site: Albany, Western Australia

The 1-day testing program began at 0615 hr on 23 November with the deployment of the beacon in ~285 m of water. Once the vessel stabilized over the beacon, the active heave compensator and the Fusion rig instrumentation were tested during mock coring exercises. Tony Muir, the Maritime Hydraulics Pte, Ltd., representative, demonstrated the seafloor landing capabilities of the active heave compensator for the drilling crew during hands-on training exercises. John Grow, the Ryan Energy Technology, Inc., representative, introduced the features and demonstrated the operation of the rig floor display to both drilling crews.

The testing exercise was completed in the early hours of the next morning. Once the drill string and beacon were recovered, the vessel sailed ~22 nmi to a prearranged rendezvous point between Breaksea Island and Bald Head at the mouth of Albany harbor. The *M/V Avon* came alongside at 0745 hr; Tony Muir, John Grow, Derryl Schroeder from the Ocean Drilling Program/Texas A&M University (ODP/TAMU), and Stefan Stan (representing Siemens) boarded the *Avon*. By 0800 hr on 24 November, the *JOIDES Resolution* was under way at full speed to the first site of Leg 187.

SITE 1152

Transit to Site

The 616-nmi transit to Site 1152 was accomplished at an average speed of 11.8 kt. The vessel rode well in a combined sea/swell of 10 ft. There was an occasional burst of wind-driven spray over the bow as the ship proceeded on a southeasterly heading. The skies were overcast with good visibility. At 0800 hr on 26 November, the vessel slowed to 6 kt while the seismic equipment was deployed. The objective was to conduct a single-channel seismic (SCS) survey across the precruise survey line. Data obtained from the survey were used to find localized sediment cover. An initial review of the seismic record suggested a sediment layer possibly 70 m thick overlying basement.

Site 1152

By noon, a north-to-south seismic line was concluded and the seismic equipment retrieved. The vessel came about and slowly approached the location. A beacon was dropped on the prospectus Global Positioning System (GPS) coordinates at 1215 hr. After the hydrophones and thrusters were extended and the vessel settled on the location, the corrected PDR depth referenced to the dual elevator stool (DES) was 5066.4 m. A nine-collar bottom-hole assembly (BHA) was made up, comprising a C-4 four-cone rotary bit, a mechanical bit release, a head sub, an outer core barrel, a top sub, a head sub, seven 8¼-in drill collars, one tapered drill collar, six 5½-in drill pipes, and one crossover sub. Although no logging was anticipated, the mechanical

bit release was affixed as a means of freeing the BHA should the drilling assembly become stuck at the bit.

Hole 1152A

Hole 1152A was spudded with the rotary core barrel (RCB) at 0830 on 27 November. The bit tagged the seafloor at 5066.4 m. Instead of coring into a sediment pond, the bit appeared to contact hard rock immediately. After RCB coring 11 m with slow penetration and high and erratic torque, we decided to again attempt to contact sediment by offsetting the vessel upcurrent of the present location. The vessel was repositioned in dynamic positioning mode ~100 m north-northeast of Hole 1152A.

Hole 1152B

Hole 1152B was spudded at 1330 hr and was washed ahead to 22.6 meters below seafloor (mbsf) where we encountered a hard contact. Rotary coring was initiated in basalt at this sub-bottom depth and advanced to 40.6 mbsf with low recovery. At this depth, the drill string stuck and stalled the top drive. The driller worked for 1.25 hr to free the drill pipe with overpulls as large as 100,000 lb to regain control of the situation. After freeing the drill string, the interval from 40.6 to 45.3 mbsf was cored with improving recovery (28%). The bit was only advanced 1 m to 46.3 mbsf when the drill string stuck again. This time the drill pipe was freed with 40,000 lb of overpull. At this juncture the hole was too unstable to deepen, so coring operations were abandoned. The bit cleared the seafloor at 1500 hr and cleared the rotary table at 2345 hr on 28 November. Concurrent with the retrieval of the drill string, the beacon was successfully recovered. After the thrusters and hydrophones were retracted and the drilling equipment secured, the vessel was under way to the next site by 0000 hr on 29 November.

Although the average recovery of the site was 12%, this provided adequate material to attain our scientific objectives. During the operations at this site, the environment was very mild for this region with vessel heave not exceeding 2 m.

SITE 1153

Transit to Site 1153

We made the 130-nmi transit to Site 1153 at an average speed of 12 kt. At 1045 hr on 29 November, the vessel slowed to 6 kt and conducted a 3.5-kHz survey across the precruise survey line. As on the first survey, the data were reviewed to verify sediment cover over basement. The data showed that the sediment cover was more than sufficient to provide lateral support for BHA.

Hole 1153A

When the survey was concluded, a beacon was dropped on the prospectus site GPS coordinates at 1200 hr. The corrected PDR depth referenced to the DES was 5592.4 m. A nine-collar BHA was made up of a new C-7 four-cone rotary bit, a mechanical bit release, a head sub, an outer core barrel, a top sub, a head sub, seven 8¼-in drill collars, one tapered drill collar, six 5½-in drill pipes, and one crossover sub. Although no logging was anticipated, the mechanical bit release was affixed to free the BHA should the drilling assembly become stuck at the bit.

Hole 1153A was spudded with the RCB at 2300 hr on 29 November. The bit tagged seafloor at 5592.4 m. The drill string was washed ahead with a core barrel in place to 267.6 mbsf, where basalt was contacted. During the process of washing ahead without coring, seven wash barrels were recovered from 26.9, 142.3, 151.9, 209.6, 233.4, 243.0, and 267.6 mbsf. The last wash barrel recovered some basaltic rock, so we began rotary coring. We experienced unstable hole conditions while washing from 243 to 268 mbsf. This condition required redrilling the bottom of the washed interval. When the drill string was pulled back to 248 mbsf, the driller noted ~40,000 lb of drag at 253 mbsf.

Prior to initiating rotary coring, the core barrel was dressed with a “whirl-pak” bag containing fluorescent microspheres as a circulating fluid contamination tracer. Before coring could be initiated at 268 mbsf, the driller had to ream the hole again from 248 to 268 mbsf. The hole was then flushed with a sepiolite mud treatment. The interval 267.6–274.9 mbsf was cored, but the hole became unstable again as 7 m of fill was encountered after we recovered the core barrel. The poor downhole conditions suggested a low probability that the hole could be deepened further, so coring was terminated. The drill string was recovered; the bit cleared the seafloor at 1030 hr and cleared the rotary table at 1630 hr on 1 December. The vessel was under way to the next site by 1900 hr on 1 December.

SITE 1154

Transit to Site 1154

The 124-nmi transit to Site 1154 took 11.5 hr at an average speed of 11 kt. At 0115 hr on 2 December, the vessel slowed to 6 kt for a SCS and 3.5-kHz survey over the site. These data indicated a similar sediment thickness as we penetrated at Site 1153 (~200 m).

Hole 1154A

After the survey we deployed a beacon on GPS coordinates ~450 m southwest of our prospectus coordinates, closer to the center of a localized sediment pond. Water depth at this site obtained by PDR was 5747.4 m. A nine-collar BHA was made up of a C-7 four-cone rotary bit, a mechanical bit release, a head sub, an outer core barrel, a top sub, a head sub, seven 8¼-in drill collars, one tapered drill collar, six 5½-in drill pipes, and one crossover sub.

We spudded Hole 1154A with the RCB at 1235 hr on 2 December. We washed ahead to 233.2 mbsf before we encountered a hard contact, presumed to be igneous basement. Rotary coring advanced the hole from 233.2 to 267.6 mbsf, with an average recovery of 27%. In an effort to increase recovery, we retrieved core barrels after advancing an average of 4.5 m. Plastic bags containing fluorescent microspheres used as microbiological tracers were deployed on Cores 187-1154A-3R, 6R, and 9R.

Coring was terminated at 34.4 m into basement. The total drill string length at this depth was 6015 m, representing a static hook load of 675,000 lb. While advancing Core 9R, the driller noted evidence of deteriorating hole conditions. As we had recovered adequate material to meet our scientific objectives, we decided to abandon Site 1154. On 4 December the bit cleared the seafloor at 1215 hr and cleared the rotary table at 1445 hr. The vessel was under way to the next site by 2130 hr.

SITE 1155

Transit to Site 1155

The 149-nmi transit to Site 1155 took just over 16 hr at an average speed of 9.1 kt. The reduced transit speed was a result of a course directly into a swell and against the Southern Ocean Current. At 1345 hr on 5 December, we began a SCS and 3.5-kHz survey. We interpreted these data to indicate that the sediment cover at this site was ~200 m thick.

Hole 1155A

When the survey was concluded, the vessel came about and slowly approached our prospectus site location. We deployed a positioning beacon on GPS coordinates at 1454 hr on 5 December. PDR water depth was 4986.4 meters below the rig floor (mbrf) (4975.4 meters below sea level [mbsl]). The nine-collar BHA employed on previous sites was made up with a new C-7 four-cone rotary bit.

We began washing down through the sediment column at Hole 1155A at 0215 hr on 6 December and encountered basement at 177.3 mbsf. We rotary cored from 177.3 to 203.5 mbsf with an average recovery of 9%. In an effort to increase recovery we retrieved core barrels after an average cored interval of 4.5 m. Fluorescent microsphere tracers were deployed in the core catchers of Cores 187-1155A-2R and 7R. After we recovered Core 7R, indications from drilling parameters (stalling top drive and high torque) suggested poor hole conditions. Hoping for better recovery, we decided to terminate this hole, offset 200 m west, and initiate a second hole. We determined the direction and magnitude of the offset based on a review of the precruise seismic data, as well as the SCS record obtained during our survey. The seismic data indicated slightly thinner sediment cover over a local basement high, and our intuition suggested there might be less rubble updip. The drill string cleared the seafloor at 0330 hr on 7 December.

Hole 1155B

At 0500 on 7 December, we began washing down to basement and started coring at 147.9 mbsf after we encountered a hard contact. We advanced Hole 1155B from 147.9 to 193.0 mbsf (Cores 187-1155B-2R to 9R) and averaged 50% recovery while coring 4.6- to 5-m intervals. We deployed microsphere tracers on Cores 2R and 9R. When we tried to recover Core 10R, the core barrel arrived on deck empty, with the core catcher fingers missing. As we had retrieved sufficient material to meet our objectives, rather than attempt to clean the hole, we decided to terminate operations and move to our next site. The bit cleared the seafloor at 2130 hr on 8 December, and the vessel was under way by 0700 hr on 9 December.

SITE 1156

Transit to Site 1156

The fifth site of Leg 187 is 47 nmi southwest of Site 1155. As a result of adverse wind and sea conditions, the voyage to Site 1156 took about 7 hr at an average speed of 6.7 kt. At 1400 hr on 9 December, the vessel's speed was reduced to 5 kt in order to deploy the SCS equipment. A faulty air line rendered the air gun inoperable, so only a 3.5-kHz survey was conducted. Our survey line crossed the precruise site survey track ~400 m north of the prospectus site where basement appeared to be somewhat shallower. Both SCS site survey data and the low-speed 3.5-kHz profile obtained on final approach to Site 1156 indicated basement was at ~200 mbsf.

Hole 1156A

When the survey was concluded at 1514 hr, we dropped a positioning beacon on the GPS coordinates at the crossing of the two survey tracks, ~400 m north of the prospectus site. Water depth was estimated, with the PDR at 4878.4 mbrf. The nine-collar BHA employed on the previous sites was made up with a new C-7 four-cone rotary bit. We initiated Hole 1156A with a RCB at 2345 hr on 9 December and washed ahead to 118.2 mbsf before reaching basement. After recovering an empty wash barrel, we cored from 118.2 to 129.6 mbsf with a recovery of 55%. We deployed fluorescent microspheres as a tracer for microbiological infiltration analysis on Core 187-1156A-3R. Because of excessive heave when recovering the last core barrel (Core 3R), we could not reenter the hole into basement, so the hole was abandoned. The drill string cleared the seafloor at 1500 hr on 10 December. We offset 200 m north of Hole 1156A to a location where seismic data indicated a somewhat thicker sediment cover for our next hole.

Hole 1156B

We began washing down at Hole 1156B at 1555 hr on 10 December and drilled ahead without incident to 181.6 mbsf before contacting basement ~60 m deeper than at Hole 1156A. The wash barrel from this interval contained 2.32 m of sediment. We recovered five rotary core

barrels from this hole, representing the interval 181.6–215.2 mbsf (Cores 187-1156B-2R to 6R), with about 30% recovery. When we retrieved the barrel containing Core 187-1156B-4R (196.8–205.9 mbsf) we discovered that the core liner had been jammed and severely twisted in the core barrel. To prevent a recurrence, we did not place plastic liners in the last two core barrels. We deployed another fluorescent microsphere tracer on Core 187-1156B-2R. Following the recovery of Core 187-1156B-6R, we decided that we had recovered enough material to reach our scientific objectives and to conclude operations. The bit cleared the seafloor at 0115 hr and the rotary table at 0845 hr on 12 December, completing operations at Site 1156.

SITE 1157

Transit to Site 1157

The sixth site of Leg 187 is 50 nmi southwest of Site 1156. Our transit took 4.3 hr at an average speed of 11.6 kt. At 1315 hr on 12 December, we slowed to 5 kt to conduct a SCS survey.

Hole 1157A

We deployed a positioning beacon about 1.6 km east of the prospectus GPS coordinates where our survey indicated a 200-m sediment thickness. Water depth at this site is 5080.4 mbrf, determined by the PDR. A new C-7 four-cone rotary bit was installed on the same nine-collar BHA used at our previous sites. We started washing through the sediment column at Hole 1157A at 2300 hr on 12 December and continued to 200.0 mbsf, where drilling conditions indicated we had reached basement. A single wash barrel was recovered, and we cored from 200.0 to 216.4 mbsf before we decided, based on poor drilling conditions and recovery, to abandon the hole. We deployed fluorescent microspheres as a tracer for microbiological infiltration analysis on Core 187-1157A-2R. The drill string cleared the seafloor at 1300 hr on 13 December; we offset 200 m west to drill Hole 1157B.

Hole 1157B

We initiated Hole 1157B by washing down to 136.6 mbsf before hitting basement. Coring continued from 136.6 to 171.0 mbsf with an average recovery of 29%. Microbiological tracers were deployed on Cores 187-1157B-2R and 9R. After ~34 m of penetration and 10 m of recovered basalt, we concluded operations at this site. The bit cleared the seafloor at 0225 hr and the rotary table at 1045 hr on 15 December.

SITE 1158

Transit to Site 1158

Because of high winds and heavy seas the 42-nmi transit from Site 1157 to Site 1158 took nearly 7 hr, and we could not deploy the geophysical gear. We dropped a positioning beacon on the prospectus site GPS coordinates at 1715 hr on 15 December. Water depth as measured by the PDR at this site is 5178.4 m. The nine-collar BHA employed on the earlier sites was made up with a new C-7 four-cone rotary bit.

Hole 1158A

We began operations by washing down through the sediment column until we contacted basement at 198.9 mbsf. The wash barrel was retrieved, and we deepened the hole by rotary coring to 213.3 mbsf. We deployed fluorescent microspheres as a tracer for microbiological infiltration analysis on Core 187-1158A-2R. Rapid penetration, high and erratic torque during drilling, and poor recovery (~6%) in the two core barrels we retrieved led to our abandoning this hole. The drill string cleared the seafloor at 1330 hr on 16 December, and we offset 200 m north, where our precruise site survey indicated thinner sediment cover.

Hole 1158B

After washing through the sediment column to 126.2 mbsf and recovering the wash barrel, we rotary cored in basement to 141.2 mbsf before unstable hole conditions forced us to abandon Hole 1158B. Microbiological tracers (microspheres) were deployed on Core 187-1158B-3R. The bit cleared the seafloor at 0545 hr on 17 December; we offset another 200 m north to attempt a third hole at this site.

Hole 1158C

We contacted basement at 108.0 mbsf in Hole 1158C and recovered the wash barrel and a single rotary core barrel (108.0–117.4 mbsf, 17% recovery) before poor hole conditions again precluded continuing operations. Microsphere tracers were deployed on Core 187-1158C-2R. Based on our experience thus far and on the recovery of sufficient material to meet our primary objectives, we chose to end operations at this site. The drill bit cleared the seafloor at 1420 hr and the rotary table at 2315 hr on 17 December.

SITE 1159

Transit to Site 1159

The eighth site of Leg 187 is 133 nmi southeast of Site 1158. We conducted a 3.5-kHz and SCS survey at ~6 kt during the entire transit. The purpose of this survey was to locate additional drilling targets on a line between Sites 1158 and 1159.

Hole 1159A

We deployed a positioning beacon on the prospectus site GPS coordinates at 2208 hr on 18 December. The PDR water depth for this site is 4515.4 mbrf. The nine-collar BHA used on the other sites was reassembled, using the same C-7 four-cone rotary bit from the previous site. We began washing through the sediment column at 0645 hr on 18 December and reached basement at 145.6 mbsf in just over 2 hr. After recovering the wash barrel (Core 187-1159A-1W), we advanced by coring from 145.6 to 173.3 mbsf (Cores 187-1159A-2R through 7R). Hole conditions deteriorated rapidly while we were drilling Core 187-1159A-7R, as indicated by a sudden increase in penetration from ~2 m/hr to >10 m/hr. We abandoned the hole when we were unable to regain our previous sub-bottom depth because of fill in the hole. Core 187-1159A-8G was recovered but represents no new penetration. The rocks recovered in this core do not appear to have been cut by the bit, and we interpret them as rubble fallen into the hole and collected during the hole cleaning attempt. A tracer of fluorescent microspheres was deployed on Core 187-1159A-2R. The drill string cleared the seafloor at 1115 hr and the rotary table at 1945 on 20 December, ending operations at this site.

SITE 1160

Transit to Site 1160

Site 1160 is 241 nmi east-northeast of Site 1159. Our average speed during the 20-hr transit was >12 kt. At 1600 hr on 21 December, we began a 7-nmi south-to-north SCS and 3.5-kHz survey across the prospectus GPS coordinates. Based on our survey, a positioning beacon was dropped ~0.7 nmi north of the prospectus GPS coordinates in order to avoid rubble that might have shed off a seamount that flanks the southern side of our operations area.

Hole 1160A

Water depth at Site 1160 was determined by the PDR to be 4636.4 mbrf. The nine-collar BHA used on earlier sites was rebuilt, and a new C-7 four-cone rotary bit was made up to a mechanical bit release. We began drilling Hole 1160A by washing down through the sediment column to 166.0 mbsf at an average penetration of 66 m/hr. When the driller noted a sharp decrease in penetration, we retrieved the wash barrel and began coring into basement. We

advanced Hole 1160A by rotary coring from 166.0 to 171.1 mbsf (Cores 187-1160A-2R and 3R) before we decided to abandon the hole because of poor drilling conditions and <10% recovery. A tracer of fluorescent microspheres was deployed on Core 187-1160-2R. The drill string was pulled free of the seafloor at 1045 hr on 22 December.

Hole 1160B

After we offset 200 m further north, we washed down through sediment at a rate of 43 m/hr to 160.1 mbsf. We rotary cored from 160.1 to 205.2 mbsf, retrieving eight cores (Cores 187-1160B-2R through 9R) with nearly 30% recovery. A tracer of fluorescent microspheres was deployed on Core 187-1160B-2R. Drilling conditions deteriorated while coring the last interval. Since we had achieved our nominal penetration depth and recovered a significant amount of core, we decided to conclude operations at Site 1160. The drill bit cleared the seafloor at 2330 hr on 23 December and the rotary table at 0545 hr on 24 December.

Cautionary Note for Postcruise Sampling

During operations at Site 1160 one of the hoses attached to the new active heave compensation system ruptured, and hydraulic fluid began streaming out of the cover that protects the hoses. This resulted in an intermittent stream of hydraulic fluid that, at times, poured onto the rig floor. This fluid flow was most pronounced when the top drive was high in the derrick (i.e., adding a new length of drill pipe to the string). Because cores are handled on the rig floor immediately after a pipe connection and the core was extracted from the core barrel while a steady rain of hydraulic fluid blanketed the core handling area, some pieces of core may have come in contact with hydraulic fluid. Since all cores were pulled from the core barrel inside a plastic liner that was not split until it was on the catwalk, the bulk of the material we recovered was protected. The only exceptions are the few pieces of core that were nestled in the core catcher, which was removed from the core barrel on the rig floor. These pieces were inspected for evidence of hydraulic fluid, and none was recognized. Nonetheless, samples from the last few centimeters of recovery from each core barrel might have been contaminated. As soon as operations were concluded at Site 1160, the hoses were disconnected, so no material recovered after Site 1160 was affected.

SITE 1161

Transit to Site 1161

The 257-nmi transit between Sites 1160 and 1161 required 33 hr at an average speed of 8 kt. We made the transit at reduced speed to repair the active heave compensator hydraulic service loop. Site 1161 is the northernmost of three potential sites located during our transit survey between Sites 1158 and 1159. At 1430 hr on 25 December, we slowed to 6 kt and conducted a

south-to-north 3.5-kHz survey over GPS coordinates of this site. At 1530 hr we dropped a positioning beacon about 1 km north of our original GPS coordinates. This position is closer to the middle of the sediment pond (our drilling target).

Hole 1161A

After the hydrophones and thrusters were extended and the vessel settled on location, the PDR referenced to the DES indicated a water depth of 5031.4 mbrf. The nine-collar BHA employed at the previous sites was reassembled with a new C-7 four-cone rotary bit and a mechanical bit release. We initiated Hole 1161A at 2330 hr on 25 December and drilled to 116.0 mbsf before contacting basement. We deepened Hole 1161A by rotary coring from 116.0 to 145.3 mbsf (Cores 187-1161A-2R to 5R) before the hole had to be abandoned because of erratic high torque, rapid penetration, and poor recovery (15%). A tracer of fluorescent microspheres was deployed on Core 187-1161A-2R. The drill string cleared the seafloor at 1315 hr on 26 December, and we offset in dynamic positioning mode 200 m north.

Hole 1161B

At Hole 1161B, we washed through 158.5 m of sediment before contacting basement and retrieving a wash barrel, which recovered a few pieces of basalt. We advanced Hole 1161B by rotary coring from 158.5 to 167.0 mbsf (Cores 187-1161B-2R and 3R, 10% recovery) with the same poor drilling conditions we experienced in the first hole. Rather than attempting to start a third hole at this site, we decided that we had recovered sufficient material at this site to meet our primary shipboard objectives and to move to our next site. We deployed a second tracer of fluorescent microspheres on Core 187-1161B-2R. The drill bit cleared the seafloor at 0045 hr and the rotary table at 0915 hr on 27 December.

SITE 1162

Transit to Site 1162

The 27-nmi south-southeast transit from Site 1161 to Site 1162 required just over 3 hr at a speed of ~8 kt. Site 1162 is the second of three new sites (surveyed on our transit between Sites 1158 and 1159) subsequently approved for drilling. Our seismic data indicated that a continuous sediment pond, >12 km long and from 300 to >400 m deep, overlay strong reflectors interpreted to be volcanic basement. To optimize our drilling target, we conducted a 21-nmi, east-to-west SCS survey across the GPS coordinates of our proposed site. A positioning beacon was dropped at 1525 hr 27 December where our seismic records indicated 200-300 m of sediment.

Hole 1162A

The PDR depth referenced to the DES at Site 1162 is 5475.4 m. The nine-collar BHA employed on the previous sites was reassembled with a new C-4 four-cone rotary bit made up to a mechanical bit release. We began Hole 1162A at 0015 on 28 December by washing down through 333.2 m of sediment and recovering a single wash barrel. Coring began when drilling conditions indicated a change from soft sediment to a harder formation. We advanced the hole by rotary coring from 333.2 to 364.6 mbsf (Cores 187-1162A-2R to 5R) with generally stable hole drilling conditions. After coring 31 m, we decided to abandon the hole because recovery was low (<10%) and the character of the recovered material indicated that we were coring down a fault zone. The predominantly cataclastic material is of very limited value in identifying the geochemical signature of the mantle source (our primary scientific objective), so the hole was terminated. As part of our continuing study on the infiltration of drilling fluid into the core, we deployed tracers of fluorescent microsphere on Cores 187-1162A-2R and 3R. The drill string cleared the seafloor at 0100 hr on 29 December, and we offset in dynamic positioning mode 200 m north.

Hole 1162B

We began drilling Hole 1162B with a wash barrel in place at 0215 hr on 29 December. After washing through 348.4 m of sediment and encountering a change in drilling conditions, we recovered the wash barrel and began rotary coring. Hole 1162B was advanced from 348.4 to 407.30 mbsf (Cores 187-1162B-2R to 11R) at an average penetration of 3 m/hr. Coring was terminated when the time we had allocated to this site during our active planning process expired, even though we had not recovered material we could interpret as basaltic basement. Nevertheless, we expect to be able to use a few basalt fragments recovered from this site with shore-based analytical tools to reach our ultimate objectives. Microsphere tracers were deployed on Cores 187-1162B-2R and 11R. The average recovery for Site 1162 was 14%.

The drill bit cleared the seafloor at 0245 hr on 31 December. During this pipe trip, the rig crew conducted the end-of-the-leg nondestructive examination of the BHA. The bit cleared the rotary table at 1345 hr on 31 December, concluding operations at this site.

SITE 1163

Transit to Site 1163

The west-northwest transit from Site 1162 to Site 1163 took about 10 hr at an average speed of 10.4 kt. At 2330 hr on 31 December, we slowed to 5 kt and ran a south-to-north SCS survey on a line 1 nmi west of and parallel to the precruise site survey track. Since the valley hosting the sediment-filled pond (our prospectus site) opened to the west, we hoped that we would find a more inviting drilling target along this line. When we could find no suitable sediment cover

along this survey track, we steered a southeasterly heading, which carried us directly over the GPS coordinates of the prospectus site. Although the sediment pond is a small target at this location, we decided that the sediment thickness was sufficient to provide lateral support for the BHA. Although the duration of the survey was only 1.6 hr and covered 8 nmi, it had the distinction of lasting from one millennium to the next.

Hole 1163A

The PDR water depth referenced to the DES at this site is 4365.4 m. The nine-collar BHA employed at the other sites was reassembled, along with a previously used hard-formation C-7 four-cone rotary bit that was still in good condition. This bit was run with a mechanical bit release. We began Hole 1163A at 1030 on 1 January by washing through ~160 m of sediment below seafloor at an average penetration of 54 m/hr. When the driller noted a hard contact, we pulled the wash barrel (Core 187-1163A-1W, 0.0 to 161.0 mbsf). We advanced Hole 1163A by rotary coring 161.0–208.1 mbsf (Cores 187-1163A-2R to 11R) with generally good drilling conditions and 33% recovery. Microsphere tracers were deployed on Core 187-1163A-2R. We terminated operations at this site when we reached our depth objective of ~50 mbsf. The drill string cleared the seafloor at 2345 hr on 2 January and the rotary table at 0700 hr on 3 January.

SITE 1164

Transit to Site 1164

We made the 51-nmi northeast transit between Sites 1163 and 1164 at average speed of 11.3 kt. At 1130 hr on 3 January, we slowed to 6 kt and ran a southwest-to-northeast SCS survey over the prospectus site to confirm sediment thickness and dropped a positioning beacon on the prospectus site GPS coordinates.

Hole 1164A

The corrected PDR depth referenced to the DES at this site is 4809.4 m. The nine-collar BHA employed at the previous sites was reassembled with a new C-4 four-cone rotary bit made up to a refurbished mechanical bit release. We initiated Hole 1164A at 2145 hr on 3 January. After washing through 138.5 m of sediment and recovering a wash barrel (Core 187-1164A-1W), we cored to 146.7 mbsf before drilling conditions forced us to abandon the hole. We recovered four cores (Cores 187-1164A-2R to 4R), although the last core was probably material recovered during our attempt to ream the hole and clear several meters of fill. A fluorescent microsphere tracer bag was deployed in the core catcher of Core 187-1164A-2R. The bit cleared the seafloor at 1115 hr, and we offset 200 m back along our survey track to the southwest.

Hole 1164B

Hole 1164B was spudded with the RCB at 1230 hr on 4 January. We washed down to 150.4 mbsf at 50 m/hr and retrieved the core barrel (Core 187-1164B-1W) when the driller noted a hard contact. We advanced the hole by rotary coring to 216.1 mbsf, recovering nine cores (Cores 187-1164B-2R to 10R). Microsphere tracers were deployed on Cores 187-1164B-2R and 10R. Hole conditions and recovery were not ideal, but we continued operations until we reached our nominal depth objective. The drill string cleared the seafloor at 0045 hr and the rotary table at 0845 on 6 January, ending operations for Leg 187.